The non-autonomous retrotransposon SVA is *trans*-mobilized by the human LINE-1 protein machinery

Julija Raiz[1], Annette Damert[1,3], Sergiu Chira[3], Ulrike Held[1,2], Sabine Klawitter[2], Matthias Hamdorf[2], Johannes Löwer[1], Wolf H. Strätling[4], Roswitha Löwer[1] and Gerald G. Schumann[1,2,*]

[1]Section PR2/Retroelements, [2]Division of Medical Biotechnology, Paul-Ehrlich-Institut, Paul-Ehrlich-Strasse 51-59, D-63225 Langen, Germany, [3]Institute for Interdisciplinary Research in Bio-Nano-Sciences, Molecular Biology Center, Babes-Bolyai-University, Cluj-Napoca, Treboniu Laurean Street 42, RO-400271 Cluj-Napoca, Romania and [4]Institut für Biochemie und Molekularbiologie, Universitätsklinikum Hamburg-Eppendorf, Martinistrasse 52, D-20246 Hamburg, Germany

ABSTRACT

SINE-VNTR-*Alu* (SVA) elements are non-autonomous, hominid-specific non-LTR retrotransposons and distinguished by their organization as composite mobile elements. They represent the evolutionarily youngest, currently active family of human non-LTR retrotransposons, and sporadically generate disease-causing insertions. Since preexisting, genomic SVA sequences are characterized by structural hallmarks of Long Interspersed Elements 1 (LINE-1, L1)-mediated retrotransposition, it has been hypothesized for several years that SVA elements are mobilized by the L1 protein machinery in *trans*. To test this hypothesis, we developed an SVA retrotransposition reporter assay in cell culture using three different human-specific SVA reporter elements. We demonstrate that SVA elements are mobilized in HeLa cells only in the presence of both L1-encoded proteins, ORF1p and ORF2p. SVA *trans*-mobilization rates exceeded pseudogene formation frequencies by 12- to 300-fold in HeLa-HA cells, indicating that SVA elements represent a preferred substrate for L1 proteins. Acquisition of an *Alu*Sp element increased the *trans*-mobilization frequency of the SVA reporter element by ~25-fold. Deletion of (CC CTCT)$_n$ repeats and *Alu*-like region of a canonical SVA reporter element caused significant attenuation of the SVA *trans*-mobilization rate. SVA *de novo* insertions were predominantly full-length, occurred preferentially in G+C-rich regions, and displayed all features of L1-mediated retrotransposition which are also observed in preexisting genomic SVA insertions.

INTRODUCTION

Three different families of non-LTR retrotransposons are actively mobilized in the human genome. These are Long Interspersed Elements 1 (LINE-1, L1), *Alu* elements (Short Interspersed Elements, SINE) and SVA (SINE-VNTR-*Alu*) elements. Their success is documented by the fact that non-LTR retrotransposons encompass ~34% of the human genome, making them the most populous group of transposable elements in the human genome (1). L1 elements are the only currently known retrotransposons in the human genome that are coding for the protein machinery required for their own mobilization. Despite the *cis*-preference (2) of L1 proteins for their own encoding RNA, RNA polymerase III transcripts [*Alu,* 7SL, U6 and hY sequences (3–6)] mutated full-length L1 RNAs (2), and cellular mRNAs [resulting in processed pseudogene formation (7–9)] were experimentally demonstrated to be *trans*-mobilized by hijacking the L1-encoded protein machinery

Since genomic preexisting insertions of the hominid-specific non-autonomous non-LTR retrotransposon SVA exhibit the classical hallmarks of L1-mediated

retrotransposition (10–12,24), SVA was also assumed to use the L1 protein machinery for its own mobilization (13). These hallmarks are: (i) insertion at a 5′-TTTT/AA-3′ consensus sequence of the L1 endonuclease recognition motif, (ii) 4- to 20-bp target site duplications (TSDs) flanking each SVA insertion, (iii) poly(A) tails of varying lengths at their 3′-ends, (iv) presence of 5′-truncated SVA insertions, (v) internal rearrangements and inversions (13–15) and (vi) 3′-transductions (16,17). SVA is a composite retrotransposon and present in about 2700 copies (12) in the human genome reference sequence. Approximately 30% of them have been integrated after the divergence of humans and chimpanzees (18). The origin of SVA elements can be traced back to the beginnings of hominid primate evolution, ~18–25 Mya. Starting at the 5′-end, a full-length SVA element is composed of a $(CCCTCT)_n$ hexamer repeat region; an *Alu*-like region consisting of two antisense *Alu* fragments and an intervening unique sequence; a variable number of tandem repeats (VNTR) region, which is made up of copies of a 36- to 42-bp sequence or of a 49- to 51-bp sequence (13), presumably derived from the SVA2 element found in Rhesus macaques and humans (19–22); and a short interspersed element of retroviral origin (SINE-R) region (22). A poly(A) tail is positioned downstream of the predicted conserved polyadenylation signal AATAAA (13). Seven different SVA variants exist in hominid genomes, including 5′- or 3′-transductions, or both 5′- and 3′- transductions (21,23). The *in vivo* retrotransposition rate of the SVA retrotransposon family was recently estimated to be one in 916 births (25).

Several observations indicate that SVA elements constitute a highly active family of hominid-specific non-LTR retrotransposons whose mobilization rate exceeds processed pseudogene formation frequencies: First, seven SVA insertions were found to be associated with disease [for review see (24)] suggesting that SVA mobilization *in vivo* is currently more efficient than the formation of high-copy pseudogenes, which have not been found to be associated with any human disease so far. Second, the identified disease-causing SVA insertions are derived from different source elements of the SVA subfamilies D, E, F and F1, and SVAs from these subfamilies are polymorphic in humans (11,12,21). It was estimated that ~40% of the SVA elements in the human genome are polymorphic (11). Also, 14 SVA insertions were recently identified in the HuRef sequence that are not present in the haploid human genome reference sequence from the HGP (25). Lastly, each mRNA pseudogene originates from primarily one source locus, while retrotransposed SVAs are derived from multiple SVA source loci (16,21).

We set out to test the hypothesis that the L1 protein machinery is mobilizing SVA elements *in trans* by establishing an SVA retrotransposition reporter assay in cell culture. We compared the rate of processed pseudogene formation with the *trans*-mobilization frequencies of two human-specific SVA elements that were identified as potential source elements. We found that SVA RNAs transcribed from the retrotransposition reporter plasmids are *trans*-mobilized 12- to 300-fold more efficiently than RNA-Pol II transcripts expressed from a pseudogene

formation reporter plasmid in HeLa-HA cells. Furthermore, we demonstrate that the hexameric $(CCCTCT)_n$ repeat/*Alu*-like region at the 5′-end of canonical SVA elements and the 3′-transduced *Alu*Sp sequence of an SVA source element have different effects on SVA retrotransposition frequencies in cell culture. Marked SVA *de novo* insertions were predominantly full-length and exhibited all structural features of L1-mediated retrotransposition that are observed in pre-existing genomic SVA insertions.

MATERIALS AND METHODS

Isolation of genomic SVA_E and SVA_{F1} elements

Based on two recent publications (26,21), we selected two potentially functional human-specific SVA elements as retrotransposition reporter elements. In order to isolate the member of the SVA subfamily E (SVA_E) that served as source element of a reported retrotransposition event into the *LDLRAP1* gene (26), we performed a BLAT search of the human genome reference sequence (hg17; May 2004), using the partially published sequence of this disease-causing SVA insertion as a query to identify its potential source element. We observed 100% identity between query sequence and genomic SVA_E element H19_27 (21). Since the human genome is polymorphic for this SVA insertion, we amplified this SVA element from a BAC clone (RP11-420K14 [AC092364] obtained from the Roswell Park Cancer Institute (Buffalo, NY, USA) via the *RZPD-Deutsches Ressourcenzentrum für Genomforschung*) by PCR using primers chrom19-gen-FW and chrom19-gen-REV (Supplementary Table S1) which are specific for the genomic sequences flanking SVA H19_27. PCRs were performed using the Expand Long Template PCR System (Roche) and controlled by sequence analyses. The resulting ~2-kb PCR product was subcloned into the pGEM-T Easy vector (Promega). Subsequent sequence analysis of the cloned PCR product revealed that the amplified SVA element harbors only 21 VNTR subunits instead of 33 VNTR subunits specified in the human genome reference sequence. This finding was confirmed by sequence analysis of three independent PCR amplifications of SVA H19_27 located on the BAC clone performed with three different primer pairs. We conclude that the nucleotide sequence of the VNTR region of SVA H19_27 on the BAC clone differs from the corresponding sequence of the human genome reference sequence. To isolate the SVA element H10_1 (21) which is a source element of the SVA subfamily F1 (SVA_{F1}) together with its 3′-flanking *Alu*Sp sequence, we amplified the corresponding genomic fragment from the BAC clone RPCIB753F0114Q [AL392107] (ImaGenes) by PCR with primers H10_1 For1 and H10_1 Rev1 (Supplementary Table S1). The resulting 4291-bp PCR product was subcloned into the pTZ57R vector (Fermentas) leading to pTZ H10_1. The subcloned PCR product was verified by sequence analyses.

Retrotransposition reporter constructs and mutant L1 protein donor plasmids

pCEPneo. The *mneoI* indicator cassette of pJM101/L1.3 (61) was PCR amplified using the primers Neo-Nhe-FW and Neo-BamHI-REV (Supplementary Table S1), and subcloned into pGEM-T Easy. Next, the *mneoI* cassette was removed by NheI/BamHI digestion and inserted into pCEP4 (Invitrogen) downstream of the CMV promoter (CMV_P) and in opposite transcriptional orientation relative to the CMV promoter (Figure 1A).

pAD3/SVA$_E$. The subcloned SVA H19_27 element was reamplified by PCR using primers CT-up-Kpn and DOWN-Δ-pA (Supplementary Table S1). The resulting fragment is devoid of the SINE-R-encoded poly-adenylation signal and was inserted between CMV_P and the *mneoI* indicator cassette of pCEPneo via KpnI/NheI. CMV_P -driven SVA transcription in pAD3/SVA$_E$ reads into the *mneo* indicator cassette to be terminated by the pCEP4-encoded SV40 polyadenylation signal.

pAD4/SVA$_E$. pAD4/SVA$_E$ differs from pAD3/SVA$_E$ in the absence of the initial 499 nt of the 5′-end of SVA H19_27 covering the $(CCCTCT)_n$ hexameric repeats and the *Alu*-like region. To generate pAD4/SVA$_E$, the reamplified SVA H19_27 fragment was digested with AlwNI and NheI. The resulting 1380-bp fragment was cloned between the CMV_P and the *mneoI* indicator cassette of pCEPneo via KpnI/blunt/AlwNI and NheI (Figure 1A).

pSC3/SVA$_{F1}$. To remove the transcriptional termination signal at the SINE-R 3′-end of SVA$_{F1}$ source element H10_1 for subsequent cloning steps, the H10_1 sequence was reamplified from pTZ H10_1 using the primer pair H10_1 For2 and H10_1 Rev2 including KpnI and NheI restriction sites, respectively (Supplementary Table S1). The resulting 3527-bp PCR product was inserted into pGEM-T Easy, excised from the resulting plasmid pGEM H10_1 by KpnI/NheI digestion, and inserted between the CMV_P and the *mneoI* indicator cassette of pCEPneo via KpnI/NheI, yielding pSC3/SVA$_{F1}$.

pSC4/SVA$_{F1}$. The synthetic oligonucleotide sequence $A_{14}TTTA_{26}$ (Generi Biotech) was fused as NheI/SpeI fragment into the NheI site of the SINE-R 3′-end of pGEM H10_1, substituting for the AATAAA-containing polyA tail at the 3′-end of the genomic SVA H10_1 element. The resulting plasmid pGEM-H10_1/ΔpA. *Alu*Sp was amplified from pTZ H10_1 using oligonucleotides H10_1 *Alu*For2 and H10_1 *Alu*Rev2 including SpeI and SalI restriction sites, respectively (Supplementary Table S1), and subcloned into pGEM-T Easy. The 389-bp SpeI/SalI *Alu*Sp fragment was fused with the 3′-end of the $A_{14}TTTA_{26}$ stretch of pGEM-H10_1/ΔpA via SpeI/SalI resulting in pGEM-H10_1+*Alu*. The 3940-bp H10_1/$A_{14}TTTA_{26}$/*Alu*Sp-fragment was inserted between CMV_P and *mneoI* cassette of pCEPneo via KpnI and NheI/SalI blunt, yielding pSC4/SVA$_{F1}$.

pJM101/L1$_{RP}$$\Delta$neo$\Delta$ORF1 (L1$_{RP}$$\Delta$ORF1). pJM101/L1$_{RP}$$\Delta$neo$\Delta$ORF1 was generated by introducing a 330-bp in-frame deletion in L1 ORF1 of pJM101/L1$_{RP}$$\Delta$neo (2). The deletion was accomplished by XhoI/SapI-restriction of pJM101/L1$_{RP}$$\Delta$neo and subsequent religation after blunt-ending.

Cell culture, SVA retrotransposition reporter assays and statistical analyses

Cell lines HeLa-JVM and HeLa-HA (28) were cultured in DMEM High Glucose (Biochrom AG, Berlin, Germany) supplemented with 10% FCS (Biowest, Nuaillé, France), 100 µg/ml streptomycin and 100 U/ml penicillin. To perform retrotransposition reporter assays with initial hygromycin selection for the presence of retrotransposition reporter plasmid and L1 protein donor plasmid, 1.8×10^6 cells were plated on 10-cm dishes or T75-flasks. Plated cells were cotransfected with 3 µg of an SVA retrotransposition reporter plasmid or pCEPneo and 3 µg of an L1 protein donor construct (pJM101/L1$_{RP}$$\Delta$neo, pJM101/L1$_{RP}$$\Delta$neo$\Delta$ORF1) or pCEP4 (negative control) using FUGENE 6 (Roche) according to the manufacturer's instructions. Each cotransfection was performed twice or thrice in quadruplicate: In each case, three cotransfections were used to quantify retrotransposition rates of the SVA reporter elements and pseudogene formation rates of the pCEPneo construct. The fourth cotransfection was used to isolate cell lysates and total RNA in order to analyze expression of retrotransposition reporter cassettes and L1-specific gene products expressed from the L1 donor plasmids. Starting 24 h post-transfection, cells were subjected to hygromycin (200 µg/ml, Invitrogen) selection for 14 days. After trypsinization and reseeding, cells were selected for L1-mediated retrotransposition events in medium containing 400 µg/ml G418 (Invitrogen). After 11–12 days of selection, G418^R colonies were either fixed an stained with Giemsa (Merck) to quantify retrotransposition events as described previously (27), or individual G418^R colonies were isolated and expanded to characterize SVA *de novo* retrotransposition events.

To perform retrotransposition reporter assays after transient cotransfection of the respective reporter plasmid and L1 donor plasmid (without hygromycin selection), 2.8×10^6 cells were plated on 15-cm dishes, and transiently cotransfected with 8 µg of the reporter plasmids pAD3/SVA$_E$, pAD4/SVA$_E$ or pCEPneo and 8 µg of either pJM101/L1$_{RP}$$\Delta$neo or pCEP4 using FUGENE 6. Each cotransfection was performed four times in parallel. HeLa cells resulting from one transient cotransfection experiment each were used to analyze the expression of ORF1p encoded by pJM101/L1$_{RP}$$\Delta$neo. Cells were trypsinized 2 days after transfection, re-seeded, and cultivated in G418 containing medium for 14 days. The *cis*-retrotransposition rate which was observed after cotransfection of pJM101/L1$_{RP}$ and pCEP4 served as positive control and was set as 100%. To obtain countable results for retrotransposition in *cis*, only 1×10^4 cells were plated for G418 selection. Transfection efficiency was determined by cotransfecting
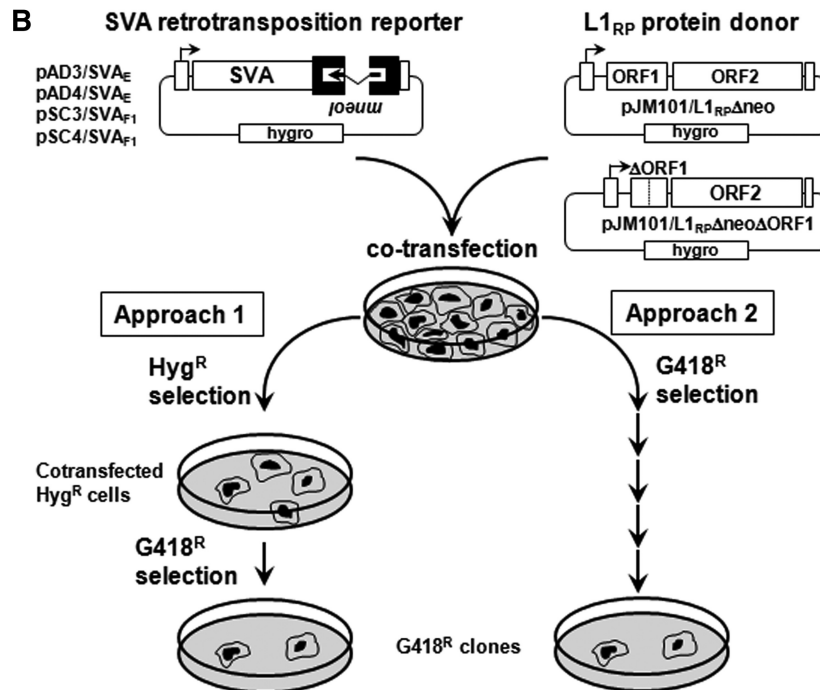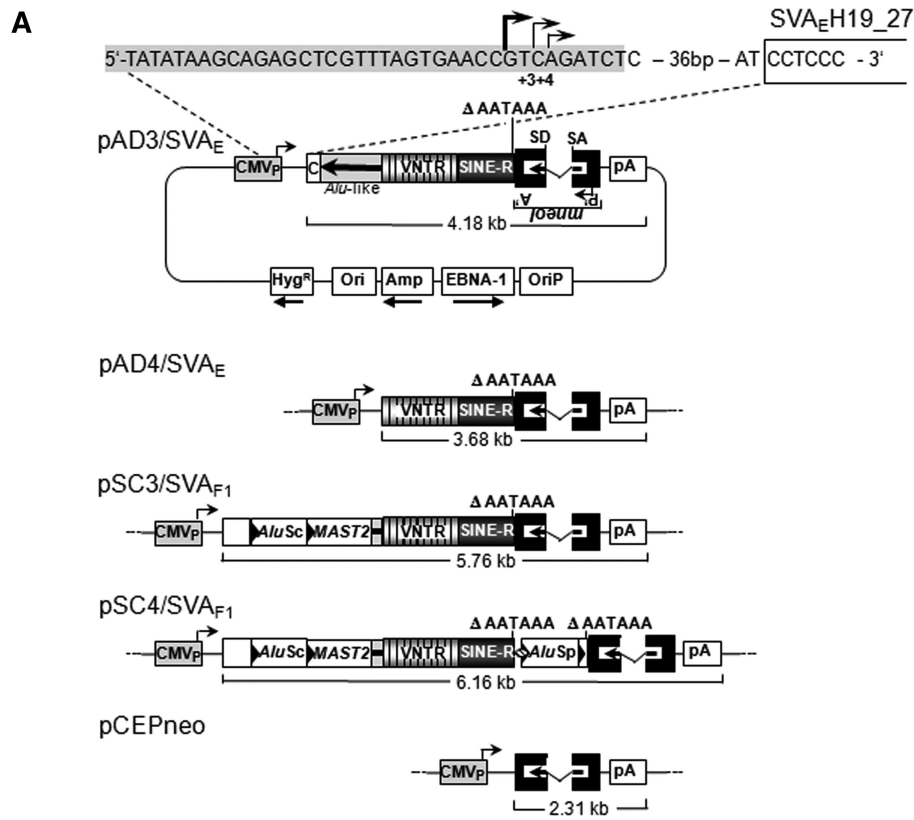
Figure 1. Rationale of the SVA *trans*-mobilization assay. (**A**) Schematic representation of SVA retrotransposition reporter plasmids, and pseudogene-formation control construct pCEPneo. SVA reporter elements in pAD3/SVA$_E$, pAD4/SVA$_E$, pSC3/SVA$_{F1}$ and pSC4/SVA$_{F1}$ and the processed pseudogene formation cassette in pCEPneo were each tagged with the indicator gene *mneoI*, and set under transcriptional control of the human CMV promoter (CMV$_P$). Splice donor (SD) and splice acceptor (SA) sites of the oppositely oriented γ-globin intron are indicated. *mneoI* is flanked by a heterologous promoter (P′) and a polyadenylation signal (A′). Transcripts originating from CMV$_P$ driving SVA *mneoI* or CEP *mneoI* transcription can splice the intron, but contain an antisense copy of the *neo* gene. G418 resistant (G418^R) colonies arise only if this transcript is reverse transcribed, integrated into chromosomal DNA, and expressed from its own promoter P′. Each SVA reporter element was inserted between CMV$_P$ and the *mneoI* cassette. pAD4/SVA$_E$, differs from pAD3/SVA$_E$ in the deletion of the initial 498 nt of the SVA 5′-end covering (CCCTCT)$_n$- and *Alu*-like region. pSC4/SVA$_{F1}$ varies from pSC3/SVA$_{F1}$ in the insertion of the 389-bp *Alu*Sp element fused to the A$_{14}$TTTA$_{26}$ stretch between

4 μg of pEGFP-N1 (Clontech), 4 μg of pAD3/SVA$_E$, pAD4/SVA$_E$ or pCEPneo and 8 μg of the L1 donor plasmid into 2.8×10^6 HeLa-JVM cells using FUGENE 6. EGFP expressing cells were counted 24 h post-transfection by flow cytometry. The percentage of green fluorescent cells was used to determine the transfection efficiency of each sample (2,29). Statistical evaluation was performed by means of an Analysis of Variance (ANOVA). To control the overall type I error α = 0.05, *P*-values were adjusted according to Dunnett for multiple comparisons. The statistical analysis was performed with SAS®/STAT software, version 9.2 SAS system for Windows.

Quantitative real-time RT-PCR

Fourteen days after cotransfection of HeLa cells with pJM101/L1$_{RP}$Δneo and either SVA retrotransposition reporter plasmid or pCEPneo, total RNA was extracted from hygromycin-selected HeLa cells using TRIZOL® (Invitrogen) following the manufacturer's instructions. One microgram of total RNA was incubated with 2 U of RNAse-free DNaseI (Invitrogen) for 30 min at room temperature. Using the *SuperScript III®* First-Strand Synthesis System for RT–PCR (Invitrogen) in combination with an oligo(dt)$_{16-18}$ primer, first-strand cDNA was synthesized from 0.5 μg of DNaseI-digested, total RNA according to the manufacturer's instructions. To quantify levels of spliced transcripts expressed from the *mneo*-tagged reporter elements in pAD3/SVA$_E$, pAD4/SVA$_E$, pSC3/SVA$_{F1}$, pSC4/SCA$_{F1}$ and pCEPneo, real-time PCR was performed in triplicate applying TaqMan® chemistry (Applied Biosystems) in an Applied Biosystems 7900HT Fast Real-Time PCR System base unit. We used a primer /probe combination (Neofor: 5′-GCTATTCGGCTATGACTGG-3′; Neorev: 5′-GCCA CGATAGCCGCGCTGC-3′; probe: 5′-FAM-CCTCGTC CTGAAGCTCATTC-3′) specifically recognizing the spliced *mneoI* cassette. For normalization, eukaryotic 18srRNA was used as internal control. Cycling conditions were as follows: 95°C for 15 min (initial cycle), 95°C for 15 s and 60°C for 1 min (40 cycles). The software applied to analyze real-time and end point fluorescence was RQ manager 1.2. Relative quantification of RNA expression was carried out using the ΔΔC_t method (30).

Immunoblot analysis

To assess L1 ORF1p and L1 ORF2p expression, HeLa cells were cotransfected as described above and harvested 14 days (with hygromycin selection) or 2 days later (without hygromycin selection), respectively. Cells were lysed in RIPA buffer (25 mM Tris, pH 8, 137 mM NaCl, 1% glycerol, 0.5% sodium deoxycholate, 1% Nonidet P-40, 2 mM EDTA, pH 8, 0.1% SDS and protease inhibitors), and lysates were cleared by centrifugation. In the case of transient cotransfection of SVA reporter plasmid and L1 protein donor, 2.8×10^6 cells were plated on 15-cm dishes and transiently cotransfected as described above. Cells of one 15-cm dish carrying the respective plasmids were trypsinized 2 days after cotransfection and lysed with RIPA lysis buffer. Twenty micrograms of each protein lysate were boiled in Laemmli buffer, loaded on 12% polyacrylamide gels, subjected to SDS–PAGE, and electroblotted onto nitrocellulose membranes. After protein transfer, membranes were blocked for 2 h at room temperature in a 10% solution of non-fat milk powder in 1× PBS-T [137 mM NaCl, 3 mM KCl, 16.5 mM Na$_2$HPO$_4$, 1.5 mM KH$_2$PO$_4$, 0.05 % Tween 20 (Sigma)], washed in 1× PBS-T, and incubated overnight with the respective primary antibody at 4°C. To detect L1 ORF1p, the polyclonal rabbit-anti-L1ORF1p antibody #984 (see Supplementary Data) was used in a 1:2000 dilution in 1× PBS-T containing 5% milk powder. L1 ORF2p expression was verified using a rabbit anti-ORF2p-N antibody (31) at a 1:1000 dilution in 1× PBS, 5% milk powder, 0.05 % Tween 20. Membranes were washed thrice in 1× PBS-T and incubated with an HRP-conjugated, secondary anti-rabbit IgG antibody (Amersham Biosciences) at a dilution of 1:30 000 in 1× PBS-T/5% milk powder for 2 h. Subsequently, the membrane was washed three times for 10 min in 1× PBS-T. ß-actin and α-tubulin expression were detected using a monoclonal anti-β-actin antibody (clone AC-74, Sigma-Aldrich) and a polyclonal anti-α-tubulin antibody (ab4074, Abcam) as primary antibodies at dilutions of 1:30 000 and 1:10 000, respectively. Anti-mouse HRP-linked species-specific antibody (from sheep) at a dilution of 1:10 000 and anti-rabbit HRP-linked specific antibody at a dilution of 1:5000 served as secondary antibodies specific for anti-β-actin and anti-α-tubulin antibody, respectively. Immunocomplexes were visualized using lumino-based ECL immunoblot reagent (Amersham Biosciences).

Analysis of SVA *de novo* insertions

Genomic DNA from expanded G418^R -HeLa colonies was isolated applying the Qiagen DNeasy® Tissue Kit according to the manufacturer's protocol. To test for the

Figure 1. Continued

SINE-R 3′-end and *mneoI* cassette. Transcriptional termination signals (ΔAATAAA) at the SINE-R 3′-end and in the sequence flanking the 3′ TSD of *Alu*Sp were omitted from the inserted SVA retrotransposition cassettes to ensure transcriptional read-through into the *mneoI* cassette and polyadenylation at the pCEP4-encoded SV40 polyadenylation signal (pA). pCEPneo is distinguished from the SVA reporter elements by the absence of any SVA sequence. CMV$_P$ sequences are highlighted in grey. CMV$_P$ major and minor transcription start sites (47) are indicated by arrows. Black rectangles, *Alu* TSDs; (**B**) Experimental setup to test for *trans*-mobilization of *mneoI*-tagged SVA elements by the L1 protein machinery. Approach 1: Hygromycin selection for the presence of SVA reporter and L1 protein expression plasmid. SVA retrotransposition reporter plasmids or pCEPneo were each cotransfected with L1 protein donor pJM101/L1$_{RP}$Δneo or pJM101/L1$_{RP}$ΔneoΔORF1 into HeLa cells which were subsequently selected for hygromycin resistance for 14 days. Resulting cell populations were assayed for retrotransposition events by selecting for 9–12 days for G418^R HeLa colonies. Approach 2: Transient cotransfection of SVA$_E$ reporter plasmids and L1 protein donor plasmid pJM101/L1$_{RP}$Δneo with subsequent G418^R selection. Two days after cotransfection of SVA reporter plasmids or pCEPneo and pJM101/L1$_{RP}$Δneo, HeLa cells were assayed for L1-mediated *trans*-mobilization of the respective reporter cassette by selection for G418 resistance.

presence of the spliced *mneo*I indicator cassette, a diagnostic PCR was performed using the intron-flanking primer pair GS86/GS87 (Figure 4 and Supplementary Table S1). PCR cycling conditions were as follows: 3 min at 96°C, (30 s at 96°C, 15 s at 56°C; 2 min at 72°C) 25 cycles, 7 min at 72°C. To determine genomic pre- and post-integration sites of SVA *de novo* insertions, we used a modified version (32) of a previously published extension primer tag selection preceding solid-phase ligation-mediated PCR (EPTS/LM-PCR) (33) to isolate 3′ junctions of these insertions. Products of the final PCR were separated in a 1% agarose gel, isolated from the gel using the QIAquick Gel Extraction Kit (Qiagen), and sequenced either directly or after subcloning into pGEM-T Easy. Obtained sequences were mapped to the human genome using the UCSC genome browser at http://genome.ucsc.edu. To characterize 5′-junctions of each SVA *de novo* insertion, primers specific for the genomic sequence adjacent to the 5′-end of the *de novo* insertions were designed. The second PCR primer used was GS87, GS88 or, alternatively, HERV-K REV because these primers bind specifically to the retrotransposed SVA$_E$ reporter cassette. All oligonucleotides used in this study are listed in Supplementary Table S1. Genomic pre-integration sites and surrounding sequences were characterized using the UCSC genome browser annotation for genes, the Repeatmasker and G+C content tracks. For localization of the integration sites to particular isochores/G+C-content regions the table published by Costantini *et al.* (34) was used.

Sequence logos

To display patterns of sequence conservation between genomic target sequences of pre-existing SVA$_E$/SVA$_F$, L1-Ta and *Alu*Ya5 elements and isolated SVA$_E$ *de novo* retrotransposition events, sequence logos were generated (Figure 6) applying the program WebLogo (35, http://weblogo.berkeley.edu/logo.cgi). We randomly picked 70 genomic target sequences of preexisting members from each of the retrotransposon subfamilies L1Hs-Ta, *Alu*Ya5 and SVA$_E$ or SVA$_F$. Genomic target sequences of L1Hs-Ta and *Alu*Ya5 elements (Supplementary Table S3) were identified from databases (L1_selection.xls; L1_TSD.txt; L1_coord_seq.txt; http://batzerlab.lsu.edu) published recently (36,37). Genomic target sequences of 70 preexisting members of the SVA subfamilies E and F (Supplementary Table S3) were determined from a recently published list of human endogenous SVA insertions (21).

RESULTS

Identification, isolation and engineering of functional human-specific SVA reporter elements

In order to test the hypothesis that SVA elements are mobilized by the L1-encoded protein machinery, we set out to establish a *trans*-mobilization assay in which potentially functional marked SVA elements are tested for retrotransposition in the presence of the overexpressed L1 protein machinery. As a first step we identified

human-specific, genomic SVA elements that were likely to be retrotransposition-competent (RC). Since sequence and/or structural characteristics of RC SVA source elements were unknown and RC SVA source elements had not been identified when we started our study, we firstly selected SVA insertions reported earlier to be the cause of single cases of genetic disorders. These SVAs were caught red-handed after they were launched from RC source elements and did not have time to accumulate disfiguring mutations in the human genome. We picked the sequence of an SVA$_E$ insertion into the *LDLRAP1* gene that caused a case of autosomal recessive hypercholesterolemia (ARH) (26), as query, and performed a BLAT search of the human genome reference sequence (hg17; May 2004) to identify the potential source element of the disease-causing insertion. We observed 100% identity between the query sequence and genomic SVA$_E$ element H19_27 (Supplementary Figure S1) which displays presence/absence polymorphism in the human genome (21). Given the sequence correlation between the ARH-causing SVA insertion and SVA H19_27, and the polymorphic state of H19_27, we concluded that either H19_27 is the source element of the disease-causing SVA insertion, or both H19_27 and the ARH-causing insertion are derived from the same source element which is not present in the analyzed human genome reference sequence. Therefore, we chose the SVA$_E$ element H19_27 as a reporter element for the planned SVA retrotransposition reporter assays. To generate the SVA retrotransposition reporter plasmid pAD3/SVA$_E$, the genomic canonical SVA$_E$ element H19_27 was amplified by PCR, tagged at its 3′-end with the *mneoI* indicator cassette (38), and inserted into the episomal pCEP4 expression vector, where the SVA reporter cassette was set under the control of the human CMV promoter (Figure 1A; see 'Materials and Methods' section). To address the question if the (CCCTCT)$_n$ repeats and/or the 300-bp *Alu*-like region at the 5′-end of SVA elements play a role in the efficiency of any potential *trans*-mobilization of SVA elements, we deleted 498 nt of the 5′-end sequence of the SVA element in pAD3/SVA$_E$ to generate pAD4/SVA$_E$ (Figures 1 and Supplementary Figure S1).

We chose the genomic SVA$_{F1}$ element H10_1 as second retrotransposition reporter, because it has been identified recently as source element of at least 13 SVA$_{F1}$ subfamily members (21,23), including one SVA$_{F1}$ element that is the progenitor of a disease-associated insertion into the *HLA-A* gene (39). The human-specific SVA$_{F1}$ subfamily was generated by the acquisition of a MAST2 sequence via splicing (21,23), includes at least 84 elements and has further evolved by usurping 5′- and 3′-transductions that include *Alu* sequences. We PCR-amplified SVA H10_1 together with its 3′-flanking functional *Alu*Sp element from a BAC clone because it was shown that, due to the weak transcriptional termination signal at the 3′-end of the SINE-R module, transcriptional readthrough into the 3′-flanking genomic *Alu*Sp sequence can occur (21) (Figure 1A). Termination of Pol II transcription by a termination signal located downstream of the *Alu*Sp TSD caused 3′-transducing H10_1 transcripts that

were retrotransposed, leading to at least 13 genomic 3′-transduced SVA_{F1} insertions (21).

Since there is evidence that both the H10_1 element alone and H10_1 derivatives including the 3′-transduced *Alu*Sp sequence have served as source elements for SVA retrotransposition (21,23), we tested both SVA_{F1} members (Figure 1A; pSC3/SVA_{F1}, pSC4/SVA_{F1}) in our *trans*-mobilization assay.

For that purpose, we first fused the entire 3.5-kb H10_1 element at its SINE-R 3′-end with the *mneoI* indicator cassette in opposite orientation, and inserted the marked SVA_{F1} reporter element into the pCEP4 expression vector, generating pSC3/SVA_{F1} (Figure 1A). Next, we fused the genomic *Alu*Sp element to the 3′-end of SVA H10_1, which resulted in a structure that also constitutes the genomic situation. The fusion was tagged with the *mneoI* indicator cassette and the entire 6.2-kb retrotransposition reporter cassette was inserted into pCEP4, resulting in pSC4/SVA_{F1} (Figure 1A). To ensure that the indicator cassette is transcribed as efficiently as the upstream SVA sequences, transcriptional termination signals located at the SINE-R 3′-end and in the sequence downstream of the *Alu*Sp 3′ TSD were removed (ΔAATAAA; Figure 1A). Since pSC3/SVA_{F1} and pSC4/SVA_{F1} differ exclusively in the presence of an intact *Alu*Sp element at the SINE-R 3′-end, we will be able to evaluate if this element plays any role in SVA *trans*-mobilization efficiency.

L1-encoded proteins facilitate retrotransposition of both SVA_E reporter elements

To evaluate if the SVA_E reporter elements are *trans*-mobilized by the L1-encoded protein machinery, we cotransfected pAD3/SVA_E and pAD4/SVA_E with the L1 protein donor plasmid pJM101/L1$_{RP}$Δneo or pCEP4 into HeLa-JVM cells (Figure 1B) because it was demonstrated that HeLa cells can efficiently accommodate and express proteins from two different expression vectors (2). Cotransfected cells were subjected to hygromycin selection for the presence of the plasmids (Figure 1B) and subsequently selected for G418 resistance. Each SVA reporter element was tagged with an antisense copy of the selectable marker gene *neo* encoding neomycin phosphotransferase, a heterologous promoter (P′), and a polyadenylation signal (A′) (Figure 1A). This arrangement ensures that G418-resistant cells ($G418^R$) will only arise if a transcript initiated from the human CMV promoter (CMV_P) driving SVA*mneoI* or CEP*mneoI* expression is spliced, reverse transcribed, reintegrated into chromosomal DNA, and expressed from promoter P′. $G418^R$ foci indicating retrotransposition of an SVA reporter cassette, could be observed only if the L1 expression plasmid was cotransfected suggesting that L1 proteins are required for SVA mobilization (Figures 2A and Supplementary Figure S3).

Next, we asked if L1 proteins prefer our reporter SVA mRNA to any other PolII transcript as substrate for *trans*-mobilization. If this was the case, *trans*-mobilization frequency of the SVA reporter element would be expected to exceed the frequency of processed pseudogene formation of a regular PolII gene. In order to determine the pseudogene formation rate, we generated the reporter plasmid pCEPneo which differs from pAD3/SVA_E exclusively by the absence of the 1876-bp SVA sequence (Figure 1A). Since transcripts expressed from the CMV_P of pCEPneo consist exclusively of the *mneoI* indicator cassette in antisense orientation and do not include any retrotransposon sequences, these transcripts should be *trans*-mobilized as frequent as random mRNAs encoded by host PolII genes. Overall, *trans*-mobilization frequencies of the pAD3/SVA_E-encoded canonical SVA element exceeded pseudogene formation of the reverse *mneoI* cassette by 2- to 5-fold whereas the 5′-truncated SVA_E cassette encoded by pAD4/SVA_E outnumbered the pseudogene formation rate by only 1- to 3-fold (Figures 2A and Supplementary Figure S3). While the differences in *trans*-mobilization rates between pAD3/SVA_E and pCEPneo were statistically significant (p1 = 0.0001), those between pAD4/SVA_E and pCEPneo were not (p2 = 0.2212). To verify that the observed differences in *trans*-mobilization rates between pAD3/SVA_E and pAD4/SVA_E are not resulting from discrepancies in mRNA production or stability between the different SVA reporter constructs, we tested for the presence of similar amounts of spliced, tagged SVA mRNAs by quantitative real-time RT–PCR (qRT–PCR) (Figure 2B). Using primer/probe combinations specifically recognizing the spliced *mneoI* reporter cassette, we quantified the relative amounts of spliced mRNA expressed from the reporter plasmids after 14 days of hygromycin selection (Figure 2B). Clearly, the observed differences in the amounts of spliced SVA reporter mRNA of 1.1-fold between pAD3/SVA_E- and pAD4/SVA_E-tranfected cells (Figure 2B) is only minor compared to the 2- to 5-fold differences in *trans*-mobilization rates (Figure 2A). Therefore, we draw the conclusion that the 498-nt fragment deleted from the 5′-end of the canonical SVA element in pAD3/SVA_E makes the 5′-truncated element in pAD4/SVA_E a somewhat less attractive substrate for *trans*-mobilization. Interestingly, although the amount of spliced pCEPneo transcripts exceeds those derived from transcription of the SVA_E reporter cassettes, *trans*-mobilization of SVA_E transcripts is still more efficient, emphasizing that SVA_E RNA is a preferred substrate for the L1 protein machinery. In order to evaluate if the observed differences in *trans*-mobilization rates can be attributed to varying L1 protein levels, we assessed L1 ORF1p and ORF2p expression in a parallel set of cotransfected hyg^R-selected HeLa cell cultures (Figure 2C). Immunoblot analysis of cell extracts isolated the day before the onset of G418 selection of the remaining cotransfected cultures, shows that comparable amounts of ORF2p are expressed in the differently cotransfected cells. Although L1 ORF1p levels are elevated in HeLa cells cotransfected with pCEPneo relative to pAD3/SVA_E- and pAD4/SVA_E-cotransfected cells, the observed *trans*-mobilization rate is the highest in cells cotransfected with pAD3/SVA_E. This indicates that the observed differences between pseudogene formation rate and SVA_E *trans*-mobilization frequencies did not result from diverse L1 protein levels.
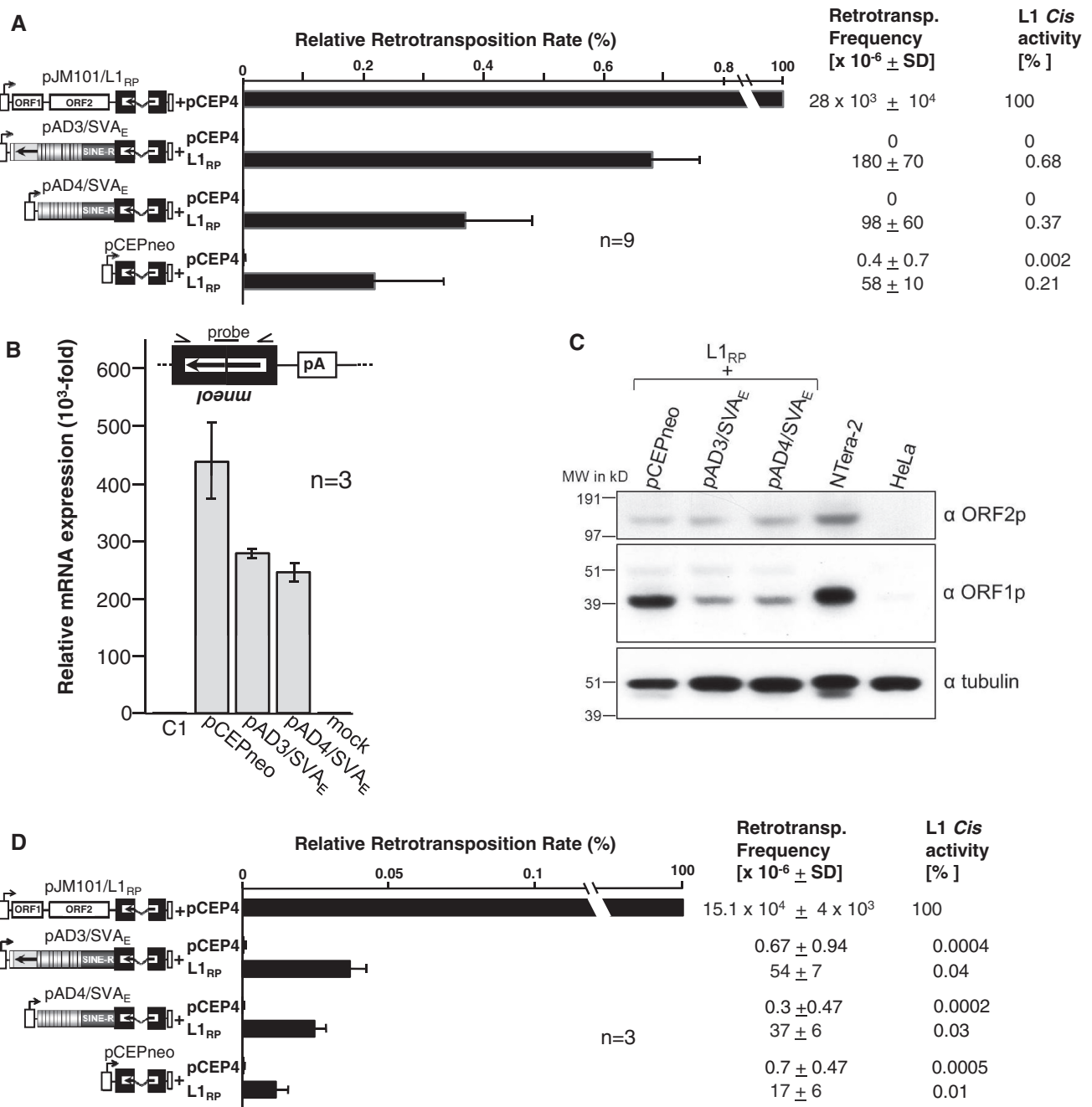
Figure 2. *Trans*-mobilization of *mneoI*-tagged SVA$_E$ reporter elements. (**A**) SVA$_E$ retrotransposition reporter assay after hygromycin selection for the presence of expression plasmids. SVA$_E$ reporter plasmids pAD3/SVA$_E$, pAD4/SVA$_E$, or pCEPneo were cotransfected with the L1 protein donor pJM101/L1$_{RP}$Δneo (L1$_{RP}$) or the empty vector pCEP4. After hyg^R selection, G418^R selection for retrotransposition events followed and retrotransposition rates were determined by counting G418^R HeLa colonies. Each cotransfection experiment and subsequent retrotransposition reporter assay was carried out three times in triplicates. Retrotransposition frequencies per 10^6 cells are listed and relative retrotransposition rates are indicated as bar diagram. *Cis* retrotransposition rate of the L1 reporter element pJM101/L1$_{RP}$ was set as 100%. Each bar depicts the arithmetic mean ± SD of the relative retrotransposition rates obtained from nine individual cotransfection experiments ($n = 9$). (**B**) qRT–PCR analyses to quantify the relative amounts of spliced transcripts expressed from retrotransposition reporter cassettes. Total RNA was isolated 48 h after cotransfection of pCEPneo, pAD3/SVA$_E$, and pAD4/SVA$_E$ with the L1 protein donor plasmid pJM101/L1$_{RP}$Δneo. The used primer/probe combination (see 'Materials and Methods' section) is specific for the spliced *mneoI*-cassette (black box with arrow). Relative amounts of mRNA expression refer to the signal obtained from total RNA of untransfected HeLa cells which was set as 1 (C1); Total RNA from mock-transfected HeLa cells served as negative control. (**C**) Immunoblot analysis of L1 protein expression in HeLa cells after cotransfection of the L1 protein donor (L1$_{RP}$) with retrotransposition reporter plasmids pAD3/SVA$_E$, pAD4/SVA$_E$ and pCEPneo. Whole-cell lysates were prepared 14 days after cotransfection upon completion of hygromycin selection and subjected to immunoblot analysis using antibodies against either L1 ORF1p (αORF1p) or L1 ORF2p (αORF2p). An amount of 20 μg of whole-cell extracts were loaded per lane. α-tubulin protein levels (∼50 kDa) were analyzed as loading control. Lysates from untransfected HeLa cells and from the germ cell tumor cell line NTera-2 served as negative and positive control for L1 protein detection, respectively. (**D**) SVA$_E$ *trans*-mobilization assay after transient cotransfection of expression plasmids. pAD3/SVA$_E$, pAD4/SVA$_E$ or pCEPneo were transiently cotransfected with pJM101/L1$_{RP}$Δneo (L1$_{RP}$) or pCEP4 into HeLa cells. Two days later, cells were G418-selected for *de novo* retrotransposition events for 14 days. G418^R HeLa colonies were Giemsa-stained and counted. Each cotransfection experiment was done in quadruplicate. Subsequent retrotransposition reporter assays were performed in triplicate. Retrotransposition frequencies per 10^6 cells are listed and relative retrotransposition rates are indicated as bar diagram. *Cis* retrotransposition rate of L1 reporter element pJM101/L1$_{RP}$ was set as 100%. Each bar depicts the arithmetic mean ± SD of the relative retrotransposition rates obtained from three individual cotransfection experiments ($n = 3$).

Next, we wanted to evaluate if we can confirm these results on *trans*-mobilization of the SVA$_E$ reporter elements in an experimental setup, in which we transiently cotransfect HeLa cells with retrotransposition reporter and L1 protein donor plasmid, and select for retrotransposition events 2 days later (Figure 1B, approach 2). In compliance with the results obtained in the case of approach 1, we observed in this transient-cotransfection setup *trans*-mobilization rates of the SVA reporter cassettes in pAD3/SVA$_E$ and pAD4/SVA$_E$ which exceeded pseudogene formation rates by 2- to 5-fold (arithmetic mean: 3.5-fold) and 1- to 3-fold (arithmetic mean: 2.4-fold), respectively (Figure 2D). Again, the difference in *trans*-mobilization rates between pAD3/SVA$_E$ and pCEPneo was statistically significant (p3 = 0.0021), whereas differences between pAD4/SVA$_E$ and pCEPneo were not (p2 = 0.0354). To test for comparable expression levels of the L1 protein machinery, we assessed L1 ORF1p expression in a parallel set of transiently cotransfected HeLa cultures. Immunoblot analysis of cell lysates harvested three days after cotransfection uncovered that there were no detectable differences in L1 ORF1p expression levels between the differently cotransfected cells (Supplementary Figure S5). This confirms that also in the transient-cotransfection setting, the observed discrepancies in *trans*-mobilization rates (Figure 2D and Supplementary Figure S4) are not a consequence of varying expression levels of the L1 protein machinery.

The 3′-transduced *Alu*Sp element increases the *trans*-mobilization rate of the SVA$_{F1}$ source element by ∼25-fold

In order to evaluate if the canonical SVA$_E$ reporter element differs in its *trans*-mobilization rate from SVA$_F$ elements that were reported to be source elements of the highly successful human-specific SVA$_{F1}$ subfamily, we tested pAD3/SVA$_E$, pSC3/SVA$_{F1}$ and pSC4/SVA$_{F1}$ (Figure 1) in our *trans*-mobilization assay in parallel. Cotransfection of pAD3/SVA$_E$, pSC3/SVA$_{F1}$ and pCEPneo with the L1 protein donor plasmid pJM101/L1$_{RP}$Δneo into HeLa-HA cells uncovered that SVA$_E$ reporter and SVA$_{F1}$ source element H10_1 are *trans*-mobilized by ∼18 and ∼12-fold relative to pseudogene formation rate, respectively (Figure 3A and B). Surprisingly, the mobilization rate of the pSC4/SVA$_{F1}$-encoded SVA$_{F1}$ source element that includes the 3′-transduced *Alu*Sp sequence was exceeding pseudogene formation rate by ∼300-fold. This corresponds with a relative retrotransposition rate of ∼11% of L1 *cis* activity (Figure 3A and B). Data suggest that the acquired *Alu*Sp sequence makes the SVA element a significantly more attractive substrate for the L1 protein machinery resulting in a mobilization rate that corresponds to *Alu*Y reporter elements (3).

SVA *trans*-mobilization requires both L1 ORF1p and L1 ORF2p

While it is obvious that the generation of G418^R foci after expression of the L1 protein machinery requires ORF2-encoded RT activity, it was unclear if L1 ORF1p

is essential for SVA *trans*-mobilization. To uncover, if L1 ORF1p is required for *trans*-mobilization of SVA elements, we generated a second L1 protein donor plasmid, termed pJM101/L1$_{RP}$ΔneoΔORF1, which differs from pJM101/L1$_{RP}$Δneo exclusively in a 330-bp in-frame deletion in L1 ORF1 (Figure 1B). The in-frame deletion of pJM101/L1$_{RP}$ΔneoΔORF1 ensures that an ORF1p mutant which lacks amino acid positions 99–208 is expressed, and that initiation of ORF2 translation within the bicistronic RNA is not perturbed. The deletion comprises the C-terminal half of the coiled coil (cc) domain and the N-terminal half of the RNA-recognition motif (RRM) domain of ORF1p (40). We confirmed by immunoblot analysis that both L1 protein donor plasmids facilitated expression of similar amounts of ORF2p after cotransfection with each of the three SVA reporter plasmids (Figures 3C). Coexpression of ORF1p deletion mutant and functional ORF2p from pJM101/L1$_{RP}$ΔneoΔORF1 did not result in *trans*-mobilization of the SVA reporter elements encoded by pAD3/SVA$_E$ and pSC3/SVA$_{F1}$ indicating that an intact ORF1p is essential for SVA retrotransposition. Surprisingly, in the absence of both overexpressed L1 proteins or ORF1p alone, *trans*-mobilization of the SVA$_{F1}$ reporter element of pSC4/SVA$_{F1}$ was still exceeding pseudogene formation by 2- to 3-fold (Figure 3A). Since the 3′-transduced *Alu*Sp sequence obviously makes the SVA RNA a preferred substrate for L1 proteins, mobilization in the absence of overexpressed L1 proteins could be explained by *trans*-mobilization of the pSC4/SVA$_{F1}$ reporter cassette beyond pseudogene formation by the moderately expressed endogenous L1 protein machinery in HeLa cells (41,42). Quantification of spliced SVA reporter RNAs by qRT–PCR (Figure 3D) and of overexpressed L1 proteins by immunoblot analysis (Figure 3C) show that the observed differences in G418^R colonies are neither a consequence of differences in the amounts of spliced retrotransposition reporter transcripts nor the result of varying amounts of overexpressed L1 proteins.

Structural features of SVA *de novo* integrants

To verify that the G418^R HeLa colonies that resulted from SVA *trans*-mobilization assays were a consequence of marked SVA *de novo* retrotransposition events, genomic DNA was extracted from 12 randomly chosen single expanded G418^R HeLa cell colonies which had resulted from cotransfection of the SVA$_E$ reporter plasmids with pJM101/L1$_{RP}$Δneo (Figure 2A). First, we carried out a diagnostic PCR on genomic DNA with primers spanning the intron of *mneoI* (Figure 4). The generation of a 792-bp PCR product shows that transcription, splicing, and L1-mediated reverse transcription of the SVA reporter elements as well as integration of the SVA$_E$-*mneoI* cDNA into the genome has occurred. A 1694-bp PCR product that would be specific for the unspliced indicator cassette encoded by the SVA$_E$ retrotransposition reporter plasmids could not be detected (Figure 4). Since PCR products obtained from HeLa clone X differed from the expected pattern, this
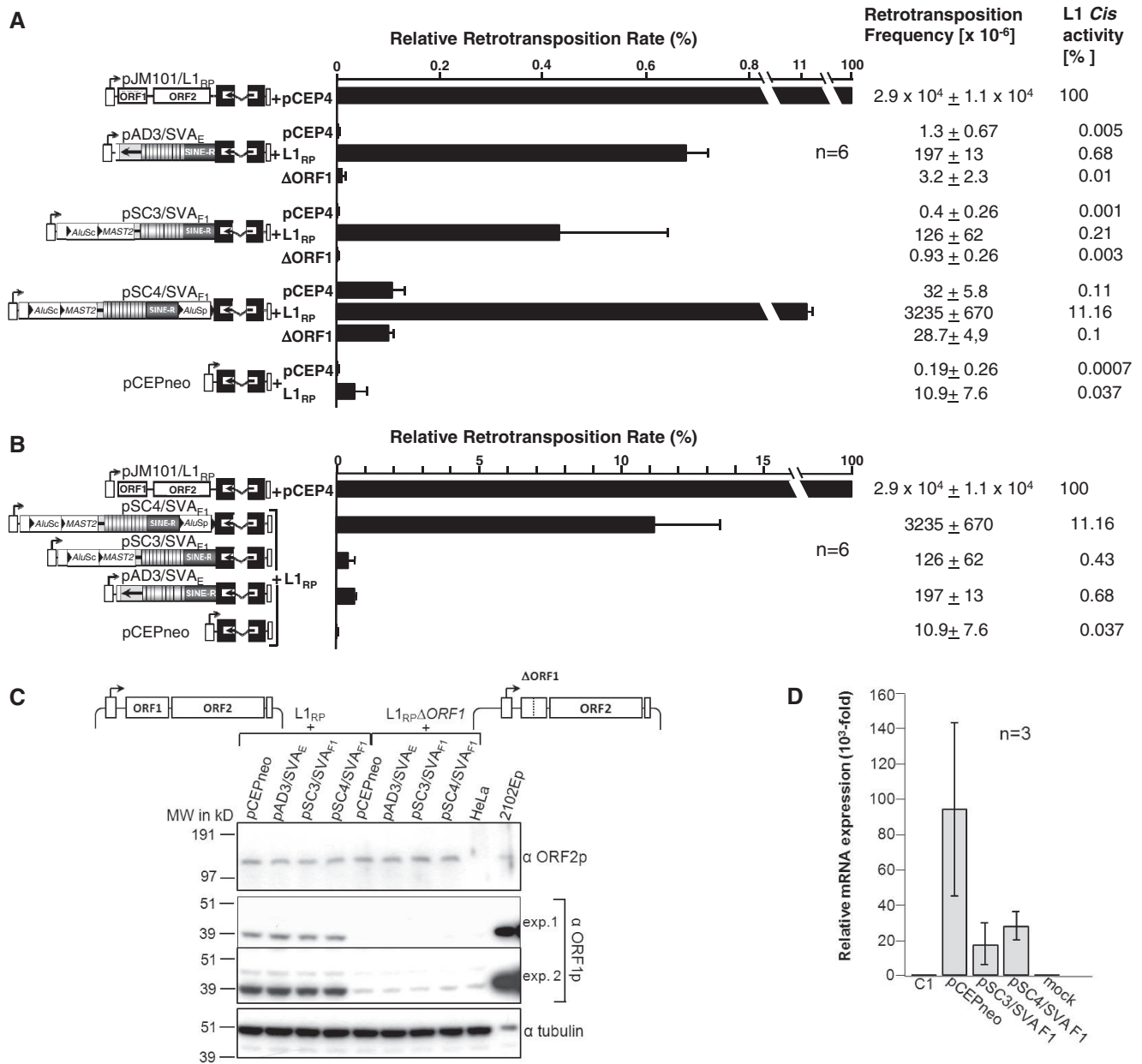
Figure 3. L1 ORF1p is required for *trans*-mobilization of SVA reporter elements. (**A**) *Trans*-mobilization of SVA_E and SVA_{F1} reporter elements in presence/absence of the entire L1 protein machinery. SVA reporter plasmids pAD3/SVA_E, pSC3/SVA_{F1} and pSC4/SVA_{F1} were each cotransfected with intact (L1_{RP}) and mutant (ΔORF1) L1 protein donor plasmid and pCEP4. pCEPneo was cotransfected with pJM101/L1_{RP}Δneo (L1_{RP}) or the empty vector pCEP4. After hyg^R selection, cotransfected HeLa cells were G418-selected for retrotransposition events and retrotransposition rates were determined. Each cotransfection experiment and subsequent retrotransposition reporter assay was carried out in triplicates twice ($n = 6$). Retrotransposition rates per 10^6 cells including standard deviations (±SD) are listed. Arithmetic means of mobilization rates relative to the *cis*-activity of pJM101/L1_{RP} (L1 *cis* activity) are specified and depicted as bar diagram. Error bars, ± SD; Primary data of *trans*-mobilization assays are summarized in Supplementary Figure S6. (**B**) The 3′ terminal *Alu*Sp sequence of SVA_{F1} element H10_1 increases its *trans*-mobilization rate by ~25-fold. For reasons of clarity, a subset of the information presented in Figure 3A is displayed. Relative retrotransposition rates (L1 *cis* activity [%]) and retrotransposition frequencies that resulted from cotransfections with the L1 protein donor pJM101/L1_{RP} (L1_{RP}) are compared. (**C**) Immunoblot analysis of L1 protein expression after cotransfection of L1 protein donors with SVA retrotransposition reporter plasmids or pCEPneo. Whole-cell lysates were prepared 14 days after cotransfection upon completion of hygromycin selection and subjected to immunoblot analysis using antibodies against either L1 ORF1p (αORF1p) or L1 ORF2p (αORF2p). An amount of 70 μg of whole-cell lysates were loaded per lane. α-tubulin protein levels (~50 kDa) were analyzed as loading control. Lysates from untransfected HeLa cells and from the germ cell tumor cell line 2102Ep served as negative and positive control for L1 protein detection, respectively. Shorter (exp.1) and longer exposures (exp.2) of the αORF1p immunoblot are presented to demonstrate expression of endogenous L1 ORF1p. (**D**) qRT–PCR analyses to quantify relative amounts of spliced transcripts encoded by the diverse retrotransposition reporter cassettes. Total RNA was isolated after 14 days of hygromycin selection following cotransfection of the reporter constructs pSC3/SVA_{F1}, pSC4/SVA_{F1} and pCEPneo with pJM101/L1_{RP}Δneo. The used primer/probe combination is specific for the spliced *mneo*I-cassette (Figure 2B). Relative amounts of mRNA expression refer to the signal obtained from total RNA of untransfected HeLa cells which was set as 1 (C1); Total RNA from mock-transfected HeLa cells served as negative control.
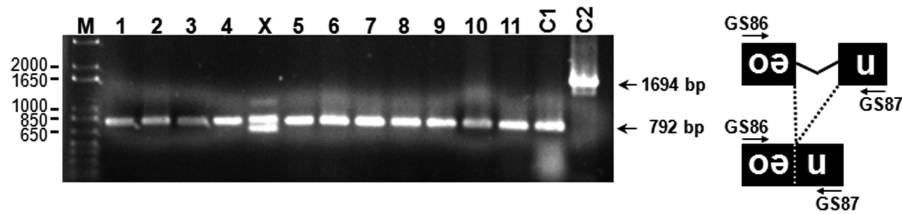
Figure 4. Diagnostic PCR to test for correct splicing of the intron from the *mneoI* indicator cassette. Genomic DNA was extracted from 12 G418[R] HeLa clones that have resulted from cotransfection of pAD3/SVA$_E$ (clones 1–8, X) or pAD4/SVA$_E$ (clones 9–11) with pJM101/L1$_{RP}\Delta$neo and subsequent hygromycin selection. The DNAs were used as template for PCR with primers GS86 and GS87. The PCR allows distinction of the spliced and reverse-transcribed form of the *mneoI* cassette (792-bp PCR product) from the original unspliced form (1694-bp PCR product) present in the reporter constructs and confirmed integration into the genome via authentic retrotransposition (29). As positive control for an unspliced *neo*[R] gene, PCR was performed on pSV2neo (BD Biosciences) mixed with genomic DNA from untransfected HeLa cells (lane C1). PCR performed on pJM101/L1$_{RP}$ DNA that was mixed with genomic HeLa DNA resulted in a fragment specific for the unspliced *neo*[R] cassette (lane C2). Lane M, 1-kb Plus DNA ladder (Invitrogen).

clone was excluded from further analyses. Next, we examined the structures of the genomic *mneo*-tagged SVA$_E$ *de novo* insertions for attributes of L1-mediated retrotransposition. Analysis of pre- and post-integration sites of eight pAD3/SVA$_E$-derived and three pAD4/SVA$_E$-derived *de novo* insertions isolated from G418[R] HeLa colonies (Figure 5) revealed that 5/11 insertions occurred into genes (Supplementary Table S2) and each insertion is indeed distinguished by structural hallmarks of L1-mediated retrotransposition such as a 30- to 78-nt poly(A) tail. The nucleotide profile of the target sites of SVA$_E$ *de novo* insertions resembles the L1 EN consensus target sequence 5′-TTTT/AA-3′ of L1-Ta *de novo* insertions and preexisting L1-Ta, *Alu*Ya5 and SVA$_{E/F}$ insertions (Figure 6). This indicates that the sequence specificity of L1 EN determines SVA integration site properties at the local level. With one exception, all characterized insertions are flanked by TSDs ranging from 8 to 19 nt (Figure 5). SVA *de novo* insertion 9 led to the formation of an 11-bp target site deletion, and the deleted sequence was replaced by a 5′-truncated *mneoI*-tagged SVA retrotransposition event lacking TSDs. The formation of similar genomic target site deletions ranging from 1 bp to >11 kb associated with 5′-truncated *de novo* insertions has been reported for EN-dependent L1 retrotransposition events earlier (43–45). Target site deletions associated with L1-mediated retrotransposition events are believed to arise as a consequence of a second-strand cleavage event that occurred upstream of the initial first-strand cleavage (43,46).

Only 2 out of the 11 characterized SVA *de novo* insertions were characterized by 5′-truncations encompassing 1716 and 680 bp (insertions 6 and 9; Figure 5), respectively. The remaining nine insertions are full-length and cover 3347 (pAD3/SVA$_E$-derived) and 2850 nt (pAD4/SVA$_E$ derived). The 5′-ends of SVA full length *de novo* insertions derived from both SVA reporter elements coincide with positions 3 or 4 downstream of the CMV promoter transcription initiation site (47) indicating that transcription of the SVA reporter elements is controlled by CMV$_P$ and not by any potential SVA-specific internal promoter. Full-length SVA *de novo* insertions include the same 44–45 nt of non-SVA sequences at their 5′-ends which result from transcriptional initiation within the CMV$_P$ region (Figure 1A).

In three cases we observed an untemplated G nucleotide between the 3′-end of the 5′ TSD and the 5′-end of full-length SVA insertions. (Figure 5A; insertions 2, 5 and 8). We identified short patches of microcomplementarity of 1–2 nt at the 5′-genomic DNA/SVA junction of 5/11 SVA *de novo* insertions which is consistent with previous studies analyzing preexisting 5′-genomic DNA/L1 junctions (48,36) and 5′-junctions of L1 *de novo* insertions (44,45). Taken together, each of the described structural features of SVA *de novo* insertions have been reported for L1 *de novo* insertions before. This is indicating that the analyzed SVA *de novo* insertions are a consequence of the *trans*-activity of the L1 protein machinery acting on SVA transcripts.

Target site preferences of *de novo* SVA integrants

SVA *de novo* insertions showed a clear integration preference for TSDs or sequences flanking endogenous non-LTR retrotransposons. Five out of the 11 characterized SVA insertions occurred into *Alu*-TSDs or adjacent sequences (Figure 5). SVA copies inserted into an L1 3′-end (insertion 10) and within the first 100 nt of the 3′-flanking region of an L1 element (insertion 5), respectively.

We calculated the average G+C content of the genomic sequences flanking *de novo* SVA insertion within 5-kb windows and 30-kb windows, and found that it amounted to 44% and 44.2%, respectively (Table 1). This was significantly higher than the genome average of 41% (p_{5kb}< 0.025; p_{30kb}< 0.005), and is in accordance with the overall distribution of preexisting members of the SVA subfamilies E and F which were reported to have accumulated in G+C-rich regions of the human genome (12). Several scenarios have been proposed for the apparent enrichment of SVA$_E$ and SVA$_F$ elements in G+C-rich regions (12). Sequence analyses of the 5-kb and 30-kb windows also indicate that SVA *de novo* insertions occurred into genomic regions with an increased *Alu* density and a relatively poor L1 density compared to the overall genomic situation (Table 1). Distribution of SVA *de novo* insertions to different isochores/ G+C-content domains of the genome is consistent with the recently
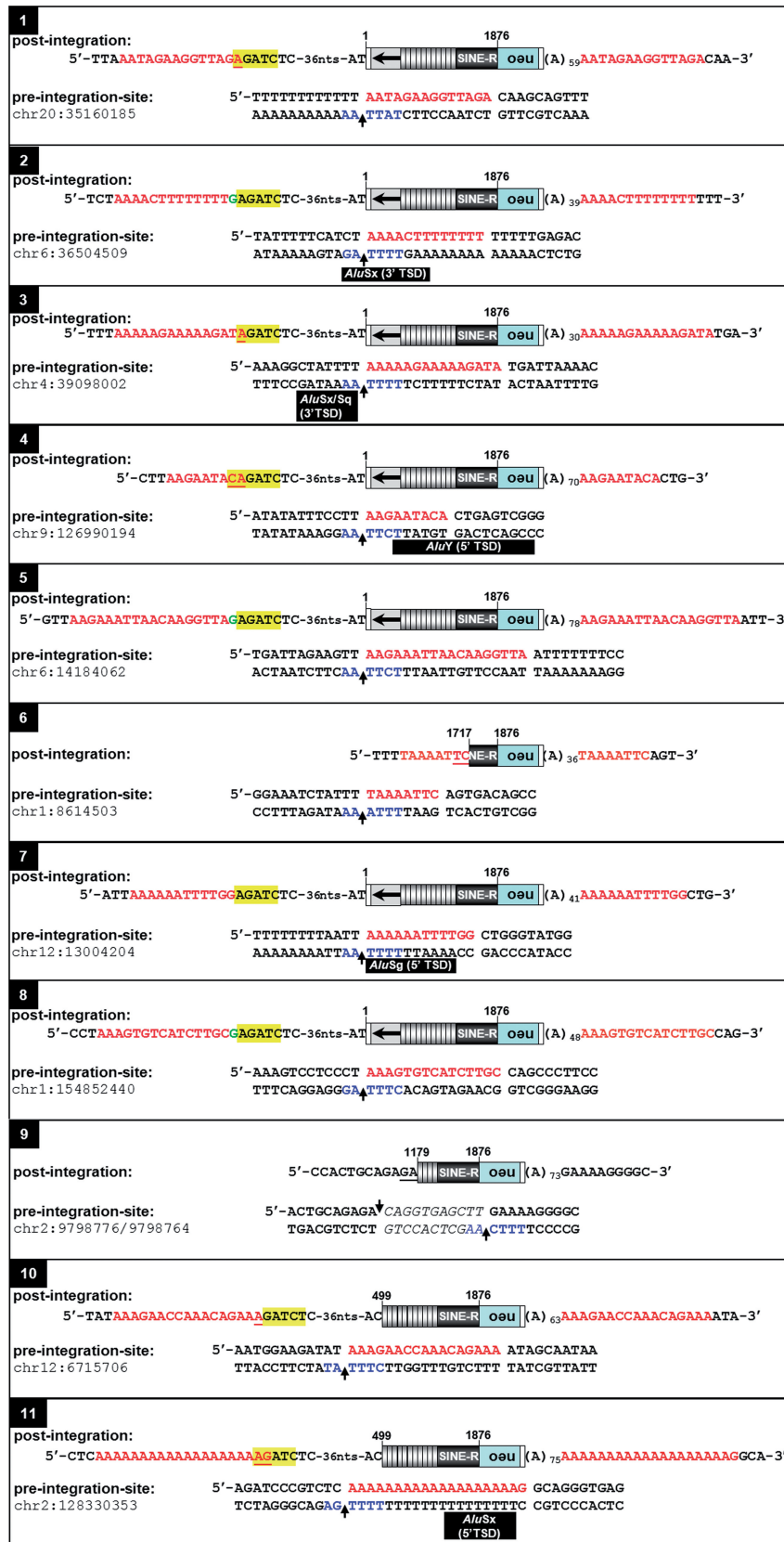
1

post-integration:
5′-TTAAATAGAAGGTTAGAGAGATCTC-36nts-AT ← SINE-R neo (A)$_{59}$AATAGAAGGTTAGACAA-3′

pre-integration-site:
chr20:35160185
5′-TTTTTTTTTTTT AATAGAAGGTTAGA CAAGCAGTTT
AAAAAAAAAAAA TTATCTTCCAATCT GTTCGTCAAA

2

post-integration:
5′-TCTAAAACTTTTTTTTGAGATCTC-36nts-AT ← SINE-R neo (A)$_{39}$AAAACTTTTTTTTTTTT-3′

pre-integration-site:
chr6:36504509
5′-TATTTTTCATCT AAAACTTTTTTTT TTTTTGAGAC
ATAAAAGTAGATTTTGAAAAAAA AAAAACTCTG
*Alu*Sx (3′ TSD)

3

post-integration:
5′-TTTAAAAAGAAAAAGATAGATCTC-36nts-AT ← SINE-R neo (A)$_{30}$AAAAAGAAAAAGATATGA-3′

pre-integration-site:
chr4:39098002
5′-AAAGGCTATTTT AAAAAGAAAAAGATA TGATTAAAAC
TTTCCGATAAAATTTTTCTTTTTCTAT ACTAATTTTG
*Alu*Sx/Sq (3′TSD)

4

post-integration:
5′-CTTAAGAATACAGATCTC-36nts-AT ← SINE-R neo (A)$_{70}$AAGAATACACTG-3′

pre-integration-site:
chr9:126990194
5′-ATATATTTCCTT AAGAATACA CTGAGTCGGG
TATATAAAGGAATTCTTATGT GACTCAGCCC
*Alu*Y (5′ TSD)

5

post-integration:
5′-GTTAAGAAATTAACAAGGTTAGAGATCTC-36nts-AT ← SINE-R neo (A)$_{78}$AAGAAATTAACAAGGTTAATT-3′

pre-integration-site:
chr6:14184062
5′-TGATTAGAAGTT AAGAAATTAACAAGGTTA ATTTTTTTCC
ACTAATCTTCAAATTCTTTAATTGTTCCAAT TAAAAAAAGG

6

post-integration:
5′-TTTTAAAATTCNE-R neo (A)$_{36}$TAAAATTCAGT-3′

pre-integration-site:
chr1:8614503
5′-GGAAATCTATTT TAAAATTC AGTGACAGCC
CCTTTAGATAAAATTTTAAG TCACTGTCGG

7

post-integration:
5′-ATTAAAAAATTTTGGAGATCTC-36nts-AT ← SINE-R neo (A)$_{41}$AAAAAATTTTGGCTG-3′

pre-integration-site:
chr12:13004204
5′-TTTTTTTTAATT AAAAAATTTTGG CTGGGTATGG
AAAAAAAATTAATTTTTTTAAAACC GACCCATACC
*Alu*Sg (5′ TSD)

8

post-integration:
5′-CCTAAAGTGTCATCTTGCGAGATCTC-36nts-AT ← SINE-R neo (A)$_{48}$AAAGTGTCATCTTGCCAG-3′

pre-integration-site:
chr1:154852440
5′-AAAGTCCTCCCT AAAGTGTCATCTTGC CAGCCCTTCC
TTTCAGGAGGGAATTTCACAGTAGAACG GTCGGGAAGG

9

post-integration:
5′-CCACTGCAGAGA SINE-R neo (A)$_{73}$GAAAAGGGGC-3′

pre-integration-site:
chr2:9798776/9798764
5′-ACTGCAGAGA *CAGGTGAGCTT* GAAAAGGGGC
TGACGTCTCT *GTCCACTCGAA*CTTTTCCCCG

10

post-integration:
5′-TATAAAGAACCAAACAGAAAGATCTC-36nts-AC SINE-R neo (A)$_{63}$AAAGAACCAAACAGAAAATA-3′

pre-integration-site:
chr12:6715706
5′-AATGGAAGATAT AAAGAACCAAACAGAAA ATAGCAATAA
TTACCTTCTATATTTCTTGGTTTGTCTTT TATCGTTATT

11

post-integration:
5′-CTCAAAAAAAAAAAAAAAAAAAGATCTC-36nts-AC SINE-R neo (A)$_{75}$AAAAAAAAAAAAAAAAAAAGGCA-3′

pre-integration-site:
chr2:128330353
5′-AGATCCCGTCTC AAAAAAAAAAAAAAAAAAAG GCAGGGTGAG
TCTAGGGCAGAGATTTTTTTTTTTTTTTTTTC CGTCCCACTC
*Alu*Sx (5′TSD)

Figure 5. Genomic SVA$_E$ *de novo* insertions display hallmarks of L1-mediated retrotransposition. Both pre- and post-integration sites are presented. Insertions 1–8 and 9–11 are derived from SVA$_E$ reporter elements encoded by pAD3/SVA$_E$ and pAD4/SVA$_E$, respectively. Nucleotide positions at the 5′-end of each SVA insertion refer to the reference sequence of SVA H19_27 [(21); Supplementary Figure S1]. Marked full-length insertions cover ∼3.3 kb (pAD3/SVA$_E$-derived) and ∼2.8 kb (pAD4/SVA$_E$-derived), respectively. Identified 5′-truncated insertions comprise 1580 bp (insertion 6) and 1620 bp (insertion 9), respectively. The L1EN cleavage site on the bottom strand is indicated in blue. Extra deoxyguanylates at the 5′-ends of *de novo* insertions are indicated in green. CMV$_P$-derived sequences are highlighted in yellow. Nucleotides representing patches of microcomplementarity are underlined. Black bars, *Alu* TSD sequences. Red lettering, SVA TSD sequences; neo, neomycin-phosphotransferase gene.
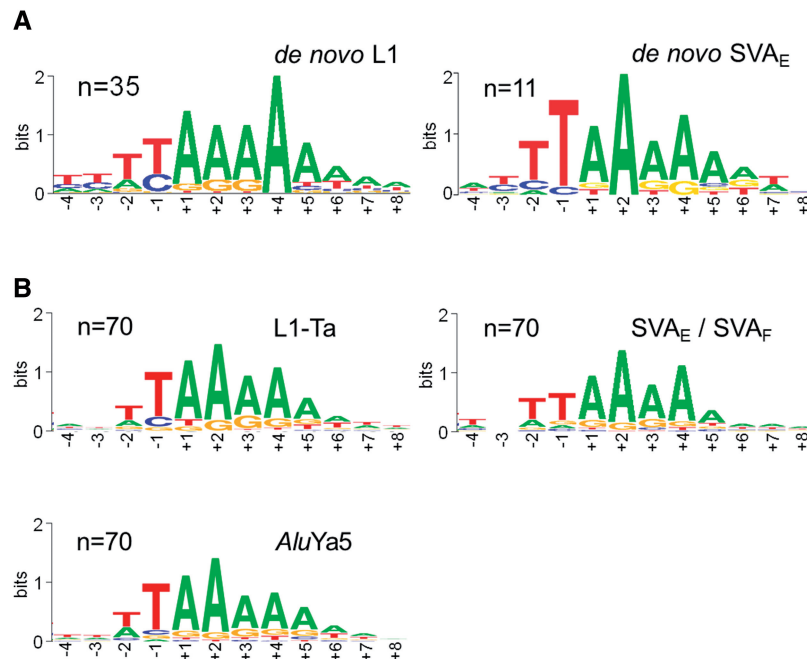
A

B

Figure 6. The nucleotide profile of SVA$_E$ *de novo* insertion sites resembles the consensus target sequence of pre-existing human-non-LTR retrotransposons. Target sequence logos were generated by multiple sequence alignments of genomic integration sites of L1Hs-Ta, *Alu*Ya5, SVA$_A$ and SVA$_E$ insertions using the program WebLogo (35). Logos for the top strand sequence cover four nucleotides of upstream and eight nucleotides of downstream sequences relative to the L1 EN cleavage site (arrow) on the bottom strand. Numbers denote nucleotide positions relative to the nicking site. (**A**) Comparison of consensus target sequences of L1 and SVA$_E$ *de novo* insertions. Target sequence logos were generated for SVA *de novo* integration sites ($n = 11$) and for target sequences of 35 L1 *de novo* insertions (43). (**B**) Target sequence logos of 70 preexisting L1-Ta, *Alu*Ya5 and SVA$_{E/F}$ insertions. Integration site sequences were identified as described in the 'Material and Methods' section.

Table 1. G+C- and retrotransposon content of genomic sequences flanking SVA *de novo* insertions

SVA insertion	G+C 5 kb (%)	*Alu* 5 kb (%)	L1 5 kb (%)	G+C 30 kb (%)	*Alu* 30 kb (%)	L1 30 kb (%)
1	46.44	35.8	1.52	43.91	45.51	7.04
2	42.40	44.54	–	42.32	31.01	9.42
3	40.57	40.86	3.58	40.54	36.62	2.74
4	48.39	39.88	–	45.98	44.36	7.88
5	38.93	13.54	22.28	42.30	16.52	6.11
6	40.03	17.34	–	38.28	11.81	–
7	39.42	36.42	11.62	42.41	19.89	1.94
8	45.43	39.92	2.66	47.02	36.46	7.30
9	50.85	13.28	–	49.17	12.26	7.28
10	44.81	29.96	24.1	48.75	31.78	5.75
11	47.00	32.98	0.48	45.42	30.25	4.19
Arith. Mean 1–11	44.02	31.32	5.21	44.19	28.77	5.97
Genome average	40.91	10.60	16.89	40.91	10.60	16.89

Analyzed sequences encompass 5-kb and 30-kb windows; G+C 5 kb/G+C 30 kb, G+C content (in percent) of 5-kb or 30-kb genomic sequence windows flanking the SVA *de novo* insertions; *Alu* 5 kb/*Alu* 30 kb (L1 5 kb/L1 30 kb), fraction of *Alu* (L1) sequences (in percent) covering 5-kb or 30-kb genomic sequence windows flanking the SVA *de novo* insertion.

described situation of genomic SVA copies (49). Eight integrants are found in isochore H1, while the remainder insertions are located in isochore L2 (two insertions) and H2 (one insertion).

DISCUSSION

L1-mediated *trans*-mobilization of SVA elements requires both L1 encoded proteins

In order to gain insight into the molecular mechanisms of the mobilization of the non-autonomous SVA elements,

we tested the hypothesis that SVA elements are *trans*-mobilized by the protein machinery encoded by functional L1 elements. We established an SVA retrotransposition reporter assay which enabled us to experimentally confirm that SVA RNA recruits the L1 protein machinery for its own mobilization. *Trans*-mobilization frequencies of the tested human-specific SVA reporter elements exceeded the processed pseudogene formation rate of cellular mRNAs by 2- to 5-fold in HeLa-JVM cells and by 12- to 300-fold in HeLa-HA cells. During the revision of this manuscript, Hancks and coworkers published in rough accordance with our results that, in their hands,

L1-mediated SVA retrotransposition exceeds processed pseudogene formation in HeLa-HA cells by 1- to 54-fold (50). We observed a strict requirement of L1 ORF1p and L1 ORF2p for the mobilization of the three tested SVA reporter elements in HeLa cells. While ORF1p was also shown to be essential for processed pseudogene formation (2,7), it is dispensable for *Alu* retrotransposition (3). The stern need for ORF1p for the mobilization of both versions of the SVA$_{F1}$ source element on chromosome 10 which differ from each other exclusively in the presence/absence of the $\sim$390 bp *Alu*Sp 3′ transduction was confirmed by Hancks *et al.* (50). However, while we also observed the same requirement of ORF1p for the mobilization of the canonical SVA$_E$ reporter element H19_27, the Kazazian laboratory obtained conflicting results when they analyzed the role of ORF1p in the mobilization of a canonical SVA$_D$ source element (50): Consistent with our findings, they reported that expression of an L1 driver with a double mutation in the RRM domain of ORF1p blocked *trans*-mobilization of the canonical SVA$_D$ source element almost entirely in HeLa-HA cells, and that coexpression of ORF2p alone with the EGFP-marked SVA$_D$ element led to barely any detectable retrotransposition events. In contrast, coexpression of ORF2p with the *mneo*I-marked SVA$_D$ element produced more G418^R foci than transfection with the intact full-length L1 driver plasmid suggesting that ORF2p alone is essential for *trans*-mobilization (50). It is unlikely that the $\sim$600-bp difference in the extension of the VNTR region between the $\sim$1.9-kb SVA$_E$ element and the $\sim$2.5-kb SVA$_D$ element played any role in the observed differences in ORF1p requirement.

Structural features of SVA elements affecting *trans*-mobilization rates

The observation that the *trans*-mobilization rates of the canonical SVA$_E$ reporter element in pAD3/SVA$_E$ exceeds retropseudogene formation by 2- to 5-fold in HeLa-JVM cells and by $\sim$18-fold in HeLa-HA cells, raises the question if potential SVA-specific structural features might qualify SVA transcripts as preferred substrates for the L1 protein machinery. First, as indicated by *Alus*, tRNA-derived SINEs (51), and tailless tRNAs, the ability of an RNA to localize to the ribosome determines its retrotranspositional success. After transcription, the SVA RNA needs to come in contact with L1 ORF2p, and out-compete the L1 RNA for the attention of ORF2p. L1 and *Alu* RNA competition for ORF2p presumably takes place at the ribosome (52,53). It has been hypothesized that the SVA-encoded *Alu*-like domain localizes SVA RNA to the ribosome by annealing with *Alu* RNAs which were suggested to be docked on ribosomes via the SRP9/14 complex (52,54). This hypothesis is consistent with our observation that the retrotransposition rate of the SVA reporter element in pAD4/SVA$_E$ which is devoid of hexameric (CCCTCT)$_n$ repeats and *Alu*-like domain, is reduced in average by 32–46% (Figure 2A and D) relative to the full-length SVA reporter element in pAD3/SVA$_E$. A potential relevance of the *Alu*-like region for *trans*-mobilization is also supported by the finding that our pSC3/SVA$_{F1}$ encoded SVA source element which also lacks the (CCCTCT)$_n$ repeats and almost the entire *Alu*-like domain exceeds pseudogene formation rate by only $\sim$12-fold while the canonical SVA$_E$ element is trans-mobilized $\sim$18-fold more efficiently than the pseudogene in HeLa-HA cells (Figure 3A and B). Second, the structures of preexisting SVA insertions imply that several modules of a canonical full-length SVA element are dispensable and not essential for successive rounds of retrotransposition. The existence of SVA2 elements which consist exclusively of VNTRs fused to short non-SVA sequences and display hallmarks of L1-mediated retrotransposition (20,21,55), suggests that the VNTR region is essential for SVA mobilization. This is supported by the fact that the VNTR region which can vary in length significantly among different SVA insertions, is the only module all mobilized SVA RNAs have in common. It was suggested that the VNTR alone or within the context of SVA may increase RNA stability (24).

We show that the 3′ transduction-mediated acquisition of the *Alu*Sp sequence by the SVA$_{F1}$ source element H10_1 (pSC4/SVA$_{F1}$) led to a 3′-transduced SVA$_{F1}$ RNA which is mobilized by the L1 protein machinery $\sim$25-fold more efficiently than the same RNA lacking the *Alu*Sp sequence (pSC3/SVA$_{F1}$) (Figure 3A and B). The relatively high *trans*-mobilization rate of the 3′-transduced SVA$_{F1}$ element H10_1 is obviously based on the observed preference of L1 proteins for SVA transcripts carrying intact *Alu*Sp sequences at their 3′-ends and is consistent with the presence of numerous genomic SVA$_{F1}$ copies characterized by the 3′-transduced *Alu*Sp sequences (21,23,39). The same mechanism hypothesized recently to be responsible for the preferential *trans*-mobilization of *Alu* elements by the L1-encoded protein machinery (3,52) could explain the favored mobilization of SVA RNAs harbouring intact *Alu* elements at their 3′-terminus (21). In this model, the *Alu* sequence is docked on ribosomes via the SRP9/14 complex and captures the L1 ORF2 protein as it is translated from an active L1 element mRNA (52). Provided that the 3′-terminal *Alu*Sp elements in SVA transcripts allow formation of the three-dimensional structure required for SRP9/14 interaction (56), *Alu* sequences could mediate docking of the respective SVA RNA to the ribosome via SRP9/14 and thus facilitate efficient capture of ORF2 proteins (3,52,54). Interestingly, the *Alu*Sc element in the 5′-region of the SVA$_{F1}$ source element (Figure 1A) does not seem to be beneficial for *trans*-mobilization, because the canonical SVA$_E$ reporter element in pAD3/SVA$_E$ which is devoid of *Alu*Sc, is mobilized at a similar frequency ($\sim$18-fold) as the SVA$_{F1}$ source element in pSC3/SVA$_{F1}$ ($\sim$12-fold) (Figure 3B).

Comparison of *trans*-mobilization rates of SVA and *Alu* elements

The *trans*-mobilization frequency of our canonical SVA$_E$ reporter element in HeLa cells after hygromycin selection equates to a relative retrotransposition rate of 0.4–0.9%

as to the *cis* retrotransposition frequency of the pJM101/L1$_{RP}$-encoded functional L1$_{RP}$ element which was set as 100% (Figures 2A and 3B). *Trans*-mobilization of the full-length SVA$_E$ reporter element exceeded pseudogene formation rates of 0.01–0.04% in HeLa-JVM and HeLa-HA cells by 2- to 5-fold and ~18-fold, respectively (Figures 2D and 3B) and coincides well with the processed pseudogene formation frequencies of 0.01–0.05% reported previously by Moran *et al.* (2). Differences in retrotransposition activity between human cell lines have been reported earlier (50) and are also known to exist between different HeLa cell lines (Moran and Deininger, personal communication). The ~25-fold increase of the *trans*-mobilization rate of the SVA$_{F1}$ source element H10_1 after the addition of the intact *Alu*Sp sequence (Figure 3) equates to a relative retrotransposition rate of ~11%. This corresponds approximately to the relative *trans*-mobilization frequency (~10%) of the *Alu*Ya5a2 NF1 element (3) which is one of the most active *Alu*s described to date (53). *Trans*-mobilization rates of the canonical SVA$_E$ reporter element (pAD3/SVA$_E$, 0.68%) and the SVA$_{F1}$ source element that lacks *Alu*Sp (pSC4/SVA$_{F1}$, 0.43%) are close to the activity of a subset of polymorphic *Alu*Y elements which were found to reach only 10% of the *Alu*Ya5a2 NF1 retrotransposition rate (53). The relative retrotransposition rates of L1, *Alu* and SVA elements determined in cell culture assays do not reflect their recently estimated *in vivo* retrotransposition rates of one in 212, 21 and 916 births, respectively (25). One possible explanation for discrepancies, for example, in the case of SVA and L1 elements, could be an excessive upregulation of SVA source element transcription in the germ line or during early stages of embryonal development relative to L1 transcription.

Hancks *et al.* (50) referred only a ≤2-fold increase in *trans*-mobilization rate of the SVA$_{F1}$ source element after acquisition of the 3′-transduced *Alu*Sp sequence and that *Alu*Y is *trans*-mobilized 30-fold more efficiently than the *Alu*Sp-including SVA$_{F1}$ element. There are several differences in the design of SVA reporter and L1 donor plasmids between the two reports which make a comparison of the presented results rather complicated. First, the 3′-transduced sequence including the *Alu*Sp element in the SVA$_{F1}$ reporter used by Hancks and coworkers (50) differed from the genomic sequence in several nucleotide substitutions which were reported to affect *trans*-mobilization rates significantly. In contrast, nucleotide sequences of all SVA reporter elements tested in our study match genomic sequences. Second, unlike Hancks *et al.*, we removed transcriptional termination signals at the SINE-R 3′-ends and in the 3′-flanking sequence of the *Alu*Sp 3′ TSD to ensure transcriptional read-through into the *mneo*I cassettes and consistent polyadenylation at the pCEP4-encoded SV40 polyadenylation signal (Figure 1A). Third, we fused the *mneo*I indicator cassette always with the 3′-end of the respective SVA reporter element, while Hancks and coworkers inserted this cassette between SINE-R and *Alu*Sp sequence of the SVA$_{F1}$ element. As a result, the transcriptional start site of the *mneo*I cassette is located ~430-bp upstream of the

3′-end of the SVA$_{F1}$ RNA, while the transcription start site of the same cassette in our analogous construct pSC3/SVA$_{F1}$ is located at the RNA 3′-end. Since 5′-truncations occur during SVA *trans*-mobilization, it could well be that the location of the indicator cassette upstream of the SVA 3′-end leads to the formation of less G418^R foci or EGFP expressing cells in cell culture assays.

SVA *de novo* insertions bear the hallmarks of mobilization by the L1 protein machinery

Analysis of pre- and post-integration sites of 11 SVA *de novo* insertions uncovered the hallmarks of L1-mediated retrotransposition. We found variable TSDs of 8–19 bp in length which correspond well to the TSD lengths of preexisting genomic L1 insertions ranging from 9 to 27 bp (15). The nucleotide profile of the target sites of the 11 analyzed SVA$_E$ *de novo* insertions resembles the L1 consensus target sequence 5′-TTTT/AA-3′ (Figure 6). SVA insertions into or next to *Alu* TSDs can be explained by the fact that their AT-rich TSDs represent recognition sequences for the L1 endonuclease in an otherwise AT-poor environment (Figure 5).

Poly(A) tail lengths of SVA *de novo* insertions (30–78 nt) exceeded those of pre-existing SVAs (2–72 nt) (21) significantly. Similar differences have been reported for L1 *de novo* insertions (3–150 nt) and preexisting L1s (approximately 13 adenosines) (43,57). One reason for the differences in polyA tail lengths between preexisting and *de novo* insertions might be the fact that each *de novo* insertion derived from an SVA$_E$ reporter cassette was polyadenylated at the sole SV40pA site present at the 3′-end of the reporter construct (Figure 1A), while RNAs derived from genomic SVA insertions are polyadenylated at sites encoded by the SINE-R region.

We found 9/11 (~82%) SVA *de novo* insertions to be full-length covering 3.35 and 2.85 kb, respectively (Figure 5 and Supplementary Table S2). Full-length insertions included the entire spliced transcript expressed from the SVA retrotransposition reporter cassette, starting with position +3 or +4 relative to the transcriptional initiation site of the CMV promoter. The fact that the percentage of 63% of preexisting full-length SVA insertions differs from the proportion of *de novo* full-length insertions could be a consequence of the relative small number of analyzed *de novo* insertions relative to the statistically more significant pool of ~2760 preexisting SVAs analyzed by Wang *et al.* (12). Since it was reported that the length of *de novo* insertions generated by L1 proteins in *trans* depends on the activity of this particular L1 element (58), the observed difference might alternatively be attributed to the use of L1$_{RP}$, one of the most active human L1 elements identified to date (59), as L1 protein donor in our reporter assays. *In vivo trans*-mobilization of genomic SVA elements, however, is probably mediated by a multitude of different functional L1 elements with most of them being less active than L1$_{RP}$ (59). Therefore, lower frequencies of endogenous full-length SVA retrotransposition events would be expected. In the case of L1, only ~6% of all *de novo* retrotransposition events (43–45) and ~5% of preexisting copies (15) are full-length.

Clearly, one reason for the significantly larger fraction of full-length SVA elements compared to L1 is the fact that L1 RT can process more of the comparatively short full-length SVA-encoded mRNAs which are only 700–4000 bp in length (12,23) than 6-kb transcripts that are encoded by full-length L1s. Since the average size of recovered L1$_{RP}$ *de novo* insertions is ∼3165 bp (44), and our *de novo* SVA full-length insertions are 3303 or 2805 bp in length (Supplementary Table S2), one would expect an increased rate of full-length SVA insertions. The fact that L1 RT successfully reverse transcribes the GC-rich VNTR region of the SVA reporter elements militates against the hypothesis that L1 5′-truncations are a consequence of an extenuated L1 RT activity. Hancks *et al.* reported that mobilization of an SVA$_E$ source element that was not under transcriptional control of an external promoter generated only 5′-truncated *de novo* insertions (50). This result suggests that SVA elements per se do not include strong promoter sequences that could facilitate full-length transcription, and that *mneo*I insertions derived from the promoterless SVA$_E$ reporter might have been produced from a cryptic promoter located upstream of the SVA sequence on the reporter plasmid. Alternatively, these SVA$_E$ insertions might not represent 5′-truncations at all and SVA transcription started within the VNTR region as numerous transcription start sites exist throughout the SVA sequence (23,50).

We found untemplated G nucleotides at the 5′-end of three full-length SVA *de novo* insertions. They have been described originally for L1 insertions (60) and were attributed to reverse transcription of the 7-methyl guanosine cap (44). Endogenous SVAs are very likely transcribed by RNA polymerase II. 5′ capping of SVA RNAs was suggested in earlier reports because of the presence of guanosine residues at the 5′-end of about 33% of pre-existing SVA insertions (12). The 5/11 insertions are characterized by short patches of microcomplementarity of 1–2 nt at the junctions between SVA 5′-end and TSD. Such short patches of microhomology were reported earlier for L1 5′ junctions (36) and indicate the involvement of double strand break repair by error-prone non homologous endjoining (NHEJ) in the attachment of the SVA 5′-end to the chromosomal DNA.

SUPPLEMENTARY DATA

Supplementary Data are available at NAR Online: Supplementary Tables 1–3, Supplementary Figures 1–6, Supplementary Methods, and Supplementary References [61–63].

ACKNOWLEDGEMENTS

FUNDING

REFERENCES

1. Lander,E.S., Linton,L.M., Birren,B., Nusbaum,C., Zody,M.C., Baldwin,J., Devon,K., Dewar,K., Doyle,M., FitzHugh,W. *et al.* (2001) Initial sequencing and analysis of the human genome. *Nature*, **409**, 860–921.
2. Wei,W., Gilbert,N., Ooi,S.L., Lawler,J.F., Ostertag,E.M., Kazazian,H.H., Boeke,J.D. and Moran,J.V. (2001) Human L1 retrotransposition: cis preference versus trans complementation. *Mol. Cell Biol.*, **21**, 1429–1439.
3. Dewannieux,M., Esnault,C. and Heidmann,T. (2003) LINE-mediated retrotransposition of marked Alu sequences. *Nat. Genet.*, **35**, 41–48.
4. Kroutter,E.N., Belancio,V.P., Wagstaff,B.J. and Roy-Engel,A.M. (2009) The RNA polymerase dictates ORF1 requirement and timing of LINE and SINE retrotransposition. *PLoS. Genet.*, **5**, e1000458.
5. Buzdin,A., Ustyugova,S., Gogvadze,E., Vinogradova,T., Lebedev,Y. and Sverdlov,E. (2002) A new family of chimeric retrotranscripts formed by a full copy of U6 small nuclear RNA fused to the 3' terminus of l1. *Genomics*, **80**, 402–406.
6. Garcia-Perez,J.L., Doucet,A.J., Bucheton,A., Moran,J.V. and Gilbert,N. (2007) Distinct mechanisms for trans-mediated mobilization of cellular RNAs by the LINE-1 reverse transcriptase. *Genome Res.*, **17**, 602–611.
7. Esnault,C., Maestre,J. and Heidmann,T. (2000) Human LINE retrotransposons generate processed pseudogenes. *Nat. Genet.*, **24**, 363–367.
8. Pavlicek,A., Paces,J., Elleder,D. and Hejnar,J. (2002) Processed pseudogenes of human endogenous retroviruses generated by LINEs: their integration, stability, and distribution. *Genome Res.*, **12**, 391–399.
9. Zhang,Z., Harrison,P. and Gerstein,M. (2002) Identification and analysis of over 2000 ribosomal protein pseudogenes in the human genome. *Genome Res.*, **12**, 1466–1482.
10. Shen,L., Wu,L.C., Sanlioglu,S., Chen,R., Mendoza,A.R., Dangel,A.W., Carroll,M.C., Zipf,W.B. and Yu,C.Y. (1994) Structure and genetics of the partially duplicated gene RP located immediately upstream of the complement C4A and the C4B genes in the HLA class III region. Molecular cloning, exon-intron structure, composite retroposon, and breakpoint of gene duplication. *J. Biol. Chem.*, **269**, 8466–8476.
11. Bennett,E.A., Coleman,L.E., Tsui,C., Pittard,W.S. and Devine,S.E. (2004) Natural genetic variation caused by transposable elements in humans. *Genetics*, **168**, 933–951.
12. Wang,H., Xing,J., Grover,D., Hedges,D.J., Han,K., Walker,J.A. and Batzer,M.A. (2005) SVA elements: a hominid-specific retroposon family. *J. Mol. Biol.*, **354**, 994–1007.
13. Ostertag,E.M., Goodier,J.L., Zhang,Y. and Kazazian,H.H. Jr (2003) SVA elements are nonautonomous retrotransposons that cause disease in humans. *Am. J. Hum. Genet.*, **73**, 1444–1451.
14. Ostertag,E.M. and Kazazian,H.H. Jr (2001) Twin priming: a proposed mechanism for the creation of inversions in L1 retrotransposition. *Genome Res.*, **11**, 2059–2065.
15. Szak,S.T., Pickeral,O.K., Makalowski,W., Boguski,M.S., Landsman,D. and Boeke,J.D. (2002) Molecular archeology of L1 insertions in the human genome. *Genome Biol.*, **3**, research0052.
16. Xing,J., Wang,H., Belancio,V.P., Cordaux,R., Deininger,P.L. and Batzer,M.A. (2006) Emergence of primate genes by

retrotransposon-mediated sequence transduction. *Proc. Natl Acad. Sci. USA*, **103**, 17608–17613.

17. Moran,J.V., DeBerardinis,R.J. and Kazazian,H.H. Jr (1999) Exon shuffling by L1 retrotransposition. *Science*, **283**, 1530–1534.

18. Mills,R.E., Bennett,E.A., Iskow,R.C., Luttig,C.T., Tsui,C., Pittard,W.S. and Devine,S.E. (2006) Recently mobilized transposons in the human and chimpanzee genomes. *Am. J. Hum. Genet.*, **78**, 671–679.

19. Jurka,J., Kapitonov,V.V., Pavlicek,A., Klonowski,P., Kohany,O. and Walichiewicz,J. (2005) Repbase Update, a database of eukaryotic repetitive elements. *Cytogenet. Genome Res.*, **110**, 462–467.

20. Han,K., Konkel,M.K., Xing,J., Wang,H., Lee,J., Meyer,T.J., Huang,C.T., Sandifer,E., Hebert,K., Barnes,E.W. *et al.* (2007) Mobile DNA in Old World monkeys: a glimpse through the rhesus macaque genome. *Science*, **316**, 238–240.

21. Damert,A., Raiz,J., Horn,A.V., Lower,J., Wang,H., Xing,J., Batzer,M.A., Lower,R. and Schumann,G.G. (2009) 5'-Transducing SVA retrotransposon groups spread efficiently throughout the human genome. *Genome Res.*, **19**, 1992–2008.

22. Ono,M., Kawakami,M. and Takezawa,T. (1987) A novel human nonviral retroposon derived from an endogenous retrovirus. *Nucleic Acids Res.*, **15**, 8725–8737.

23. Hancks,D.C., Ewing,A.D., Chen,J.E., Tokunaga,K. and Kazazian,H.H. Jr (2009) Exon-trapping mediated by the human retrotransposon SVA. *Genome Res.*, **19**, 1983–1991.

24. Hancks,D.C. and Kazazian,H.H. Jr (2010) SVA retrotransposons: Evolution and genetic instability. *Semin. Cancer Biol.*, **20**, 234–245.

25. Xing,J., Zhang,Y., Han,K., Salem,A.H., Sen,S.K., Huff,C.D., Zhou,Q., Kirkness,E.F., Levy,S., Batzer,M.A. *et al.* (2009) Mobile elements create structural variation: analysis of a complete human genome. *Genome Res.*, **19**, 1516–1526.

26. Wilund,K.R., Yi,M., Campagna,F., Arca,M., Zuliani,G., Fellin,R., Ho,Y.K., Garcia,J.V., Hobbs,H.H. and Cohen,J.C. (2002) Molecular mechanisms of autosomal recessive hypercholesterolemia. *Hum. Mol. Genet.*, **11**, 3019–3030.

27. Moran,J.V., Holmes,S.E., Naas,T.P., DeBerardinis,R.J., Boeke,J.D. and Kazazian,H.H. Jr (1996) High frequency retrotransposition in cultured mammalian cells. *Cell*, **87**, 917–927.

28. Hulme,A.E., Bogerd,H.P., Cullen,B.R. and Moran,J.V. (2007) Selective inhibition of Alu retrotransposition by APOBEC3G. *Gene*, **390**, 199–205.

29. Ostertag,E.M., Prak,E.T., DeBerardinis,R.J., Moran,J.V. and Kazazian,H.H. Jr (2000) Determination of L1 retrotransposition kinetics in cultured cells. *Nucleic Acids Res.*, **28**, 1418–1423.

30. Livak,K.J. and Schmittgen,T.D. (2001) Analysis of relative gene expression data using real-time quantitative PCR and the $2(-\Delta \Delta C(T))$ Method. *Methods*, **25**, 402–408.

31. Goodier,J.L., Ostertag,E.M., Engleka,K.A., Seleme,M.C. and Kazazian,H.H. Jr (2004) A potential role for the nucleolus in L1 retrotransposition. *Hum. Mol. Genet.*, **13**, 1041–1048.

32. Kirilyuk,A., Tolstonog,G.V., Damert,A., Held,U., Hahn,S., Lower,R., Buschmann,C., Horn,A.V., Traub,P. and Schumann,G.G. (2008) Functional endogenous LINE-1 retrotransposons are expressed and mobilized in rat chloroleukemia cells. *Nucleic Acids Res.*, **36**, 648–665.

33. Schmidt,M., Hoffmann,G., Wissler,M., Lemke,N., Mussig,A., Glimm,H., Williams,D.A., Ragg,S., Hesemann,C.U. and von,K.C. (2001) Detection and direct genomic sequencing of multiple rare unknown flanking DNA in highly complex samples. *Hum. Gene Ther.*, **12**, 743–749.

34. Costantini,M., Clay,O., Auletta,F. and Bernardi,G. (2006) An isochore map of human chromosomes. *Genome Res.*, **16**, 536–541.

35. Crooks,G.E., Hon,G., Chandonia,J.-M. and Brenner,S.E. (2004) WebLogo: A sequence logo generator. *Genome Res.*, **14**, 1188–1190.

36. Zingler,N., Willhoeft,U., Brose,H.P., Schoder,V., Jahns,T., Hanschmann,K.M., Morrish,T.A., Lower,J. and Schumann,G.G. (2005) Analysis of 5' junctions of human LINE-1 and Alu retrotransposons suggests an alternative model for 5'-end attachment requiring microhomology-mediated end-joining. *Genome Res.*, **15**, 780–789.

37. Otieno,A.C., Carter,A.B., Hedges,D.J., Walker,J.A., Ray,D.A., Garber,R.K., Anders,B.A., Stoilova,N., Laborde,M.E., Fowlkes,J.D. *et al.* (2004) Analysis of the human *Alu* Ya-lineage. *J. Mol. Biol.*, **342**, 109–118.

38. Freeman,J.D., Goodchild,N.L. and Mager,D.L. (1994) A modified indicator gene for selection of retrotransposition events in mammalian cells. *Biotechniques*, **17**, 46, 48–49, 52.

39. Takasu,M., Hayashi,R., Maruya,E., Ota,M., Imura,K., Kougo,K., Kobayashi,C., Saji,H., Ishikawa,Y., Asai,T. *et al.* (2007) Deletion of entire HLA-A gene accompanied by an insertion of a retrotransposon. *Tissue Antigens*, **70**, 144–150.

40. Khazina,E. and Weichenrieder,O. (2009) Non-LTR retrotransposons encode noncanonical RRM domains in their first open reading frame. *Proc. Natl Acad. Sci. USA*, **106**, 731–736.

41. Belancio,V.P., Roy-Engel,A.M., Pochampally,R.R and Deininger,P. (2010) Somatic expression of LINE-1 elements in human tissues. *Nucleic Acids Res.*, **38**, 3909–3922.

42. Comeaux,M.S., Roy-Engel,A.M., Hedges,D.J. and Deininger,P.L. (2009) Diverse *cis* factors controlling Alu retrotransposition: What causes Alu elements to die? *Genome Res.*, **19**, 545–555.

43. Gilbert,N., Lutz-Prigge,S. and Moran,J.V. (2002) Genomic deletions created upon LINE-1 retrotransposition. *Cell*, **110**, 315–325.

44. Gilbert,N., Lutz,S., Morrish,T.A. and Moran,J.V. (2005) Multiple fates of L1 retrotransposition intermediates in cultured human cells. *Mol. Cell Biol.*, **25**, 7780–7795.

45. Symer,D.E., Connelly,C., Szak,S.T., Caputo,E.M., Cost,G.J., Parmigiani,G. and Boeke,J.D. (2002) Human l1 retrotransposition is associated with genetic instability in vivo. *Cell*, **110**, 327–338.

46. Ichiyanagi,K. and Okada,N. (2008) Mobility pathways for vertebrate L1, L2, CR1, and RTE clade retrotransposons. *Mol. Biol. Evol.*, **25**, 1148–1157.

47. Isomura,H., Stinski,M.F., Kudoh,A., Nakayama,S., Murata,T., Sato,Y., Iwahori,S. and Tsurumi,T. (2008) A cis element between the TATA Box and the transcription start site of the major immediate-early promoter of human cytomegalovirus determines efficiency of viral replication. *J. Virol.*, **82**, 849–858.

48. Martin,S.L., Li,W.L., Furano,A.V. and Boissinot,S. (2005) The structures of mouse and human L1 elements reflect their insertion mechanism. *Cytogenet. Genome Res.*, **110**, 223–228.

49. Pozzoli,U., Menozzi,G., Fumagalli,M., Cereda,M., Comi,G.P., Cagliani,R., Bresolin,N. and Sironi,M. (2008) Both selective and neutral processes drive GC content evolution in the human genome. *BMC. Evol. Biol.*, **8**, 99.

50. Hancks,D.C., Goodier,J.L., Mandal,P.K., Cheung,L.E. and Kazazian,H.H. Jr (2011) Retrotransposition of marked SVA elements by human L1s in cultured cells. *Hum.Mol.Genet.*, **20**, 3386–3400.

51. Okada,N., Hamada,M., Ogiwara,I. and Ohshima,K. (1997) SINEs and LINEs share common 3' sequences: a review. *Gene*, **205**, 229–243.

52. Boeke,J.D. (1997) LINEs and Alus–the polyA connection. *Nat. Genet.*, **16**, 6–7.

53. Bennett,E.A., Keller,H., Mills,R.E., Schmidt,S., Moran,J.V., Weichenrieder,O. and Devine,S.E. (2008) Active Alu retrotransposons in the human genome. *Genome Res.*, **18**, 1875–1883.

54. Mills,R.E., Bennett,E.A., Iskow,R.C. and Devine,S.E. (2007) Which transposable elements are active in the human genome? *Trends Genet.*, **23**, 183–191.

55. Jurka,J. (2000) Repbase update: a database and an electronic journal of repetitive elements. *Trends Genet.*, **16**, 418–420.

56. Weichenrieder,O., Wild,K., Strub,K. and Cusack,S. (2000) Structure and assembly of the *Alu* domain of the mammalian signal recognition particle. *Nature*, **408**, 167–173.

57. Ovchinnikov,I., Troxel,A.B. and Swergold,G.D. (2001) Genomic characterization of recent human LINE-1 insertions: evidence supporting random insertion. *Genome Res.*, **11**, 2050–2058.

58. Farley,A.H., Luning Prak,E.T. and Kazazian,H.H. Jr (2004) More active human L1 retrotransposons produce longer insertions. *Nucleic Acids Res.*, **32**, 502–510.

59. Brouha,B., Schustak,J., Badge,R.M., Lutz-Prigge,S., Farley,A.H., Moran,J.V. and Kazazian,H.H. Jr (2003) Hot L1s account for the

bulk of retrotransposition in the human population. *Proc. Natl Acad. Sci. USA*, **100**, 5280–5285.

60. Lavie,L., Maldener,E., Brouha,B., Meese,E.U. and Mayer,J. (2004) The human L1 promoter: variable transcription initiation sites and a major impact of upstream flanking sequence on promoter activity. *Genome Res.*, **14**, 2253–2260.

61. Sassaman,D.M., Dombroski,B.A., Moran,J.V., Kimberland,M.L., Naas,T.P., DeBerardinis,R.J., Gabriel,A., Swergold,G.D. and Kazazian,H.H. Jr (1997) Many human L1 elements are capable of retrotransposition. *Nat. Genet.*, **16**, 37–43.

62. Waterborg,J.H. and Matthews,H.R. (1994) The electrophoretic elution of proteins from polyacrylamide gels. *Methods Mol. Biol.*, **32**, 169–175.

63. Kimberland,M.L., Divoky,V., Prchal,J., Schwahn,U., Berger,W. and Kazazian,H.H. Jr (1999) Full-length human L1 insertions retain the capacity for high frequency retrotransposition in cultured cells. *Hum. Mol. Genet.*, **8**, 1557–1560.